Molecular Dynamics of adsorbed polymer thin films using NMR Field Cycling Relaxometry

Von der Fakultät für Mathematik, Informatik und Naturwissenschaften der RWTH Aachen University zur Erlangung des akademischen Grades eines Doktors der Naturwissenschaften genehmigte Dissertation

vorgelegt von

M.Sc. Santhosh Kumar Ayalur-Karunakaran

aus Chennai, India

Berichter: Universitätsprofessor Prof.Dr.Dr.h.c. Bernhard Blümich
Universitätsprofessor Prof.Dr.rer.nat.habil Siegfried Stapf

Tag der mündlichen Prüfung: 16.07.2010

Contents

List of Figures

List of Tables

List of Symbols and Abbreviations

AFM Atomic force microscopy

B Magnetic field / induction vector

b Kuhn length

$\mathbf{B}_0$ Static magnetic field vector

$\mathbf{B}_i$ Static magnetic field vector in ith direction(i=x,y,z)

$\mathbf{B}_1$ Radio-frequency magnetic field in the rotating frame

$\mathbf{B}_{aq}$ Acquisition (magnetic) field

$\mathbf{B}_d$ Detection (magnetic) field

$\mathbf{B}_{loc}$ Local (magnetic) field

$\mathbf{B}_p$ Polarization (magnetic) field

$\mathbf{B}_r$ Relaxation (magnetic) field

$\mathbf{B}_{rf}$ Radio-frequency magnetic field

CPMG Carr-Purcell-Meiboom-Gill

DQ Double quantum

FFC Fast-field cycling

$\boldsymbol{fi}$ Interaction-specific constants

FID Free induction decay

$\mathbf{G}\tau$ Autocorrelation function of orientation

$\mathbb{G}(\tau)$ Reduced autocorrelation function

$G_{(k)}(\boldsymbol{i})$ Correlation function for component i, i=A,B or C

$\mathbb{I}(\omega)$ Reduced intensity function

$\mathbf{I}$ (ω) Spectral density function

k Constant for reproducible field transition

$\mathbf{k}_B$ Boltzmann constant

M Magnetization vector

$\mathbf{M}_0$ Thermodynamic equilibrium magnetization

$\mathbf{M}_c$ Critical molecular weight

MOSFET Metal-oxide semiconductor field-effect transistor

$\mathbf{M}_w$ Molecular weight

$\overline{M_w}$ Weight-averaged molecular weight

$\overline{M_n}$ Number-averaged molecular weight

N degree of polymerisation/number of Kuhn segments

NMR Nuclear magnetic resonance

NP Non-polarized sequence

NSE Neutron spin-echo O(k) Spin-operator functions

PB Polybutadiene

PDMS Polydimethylsiloxane

PI Polyisoprene

PP Pre-polarized sequence/Polypropylene

PS Polystyrene

Q Quality factor of the coil

$\boldsymbol{r}$ Internuclear distance

rf Radio frequency

rms Root mean square

S/N Signal-to-noise

SANS Small angle neutron scattering

$\mathbf{S}_D Q$ Double-quantum signal

T Absolute temperature

$\mathbf{T}_0$ Reference temperature

$\mathbf{T}_1$ Spin-lattice relaxation time

$\mathbf{T}_{1\rho}$ Spin-lattice relaxation time in the rotating frame

$\mathbf{T}_2$ Transverse relaxation time

$\mathbf{T}_g$ Glass transition temperature

$\mathbf{T}_m$ Melting temperature

x, y, z Components of the vector

x', y', z' Axes for the rotating frame coordinate system

ϵ Reciprocal noise level of the receiver electronics

γ Value of the exponent in the power-law relation

γ_n Gyromagnetic ratio of the nuclei 'n'

η Asymmetry parameter, in the longitudinal relaxation rate

η Filling factor

μ_0 Magnetic field constant

ω_0 Larmor frequency

τ_c Correlation time

τ_s segmental reorientation time

τ_{swt} Switching time

τ_t Terminal chain relaxation time

$\overline{\omega}_d$ Averaged coupling constant

Chapter 1

Introduction

Over the recent years, research on thin films, motivated by both the need for developing materials for new applications as well as for a fundamental understanding of the properties has greatly advanced thin film science and technology. Some of the main questions concerns the changes in the properties compared to the bulk, such as chain conformation, chain density, and accompanying effects such as altered glass transition, diffusivity, segmental relaxation etc. All these effects are far from well understood and investigations from various corners of research are needed for a better understanding of dynamics in these systems.

Conventionally, polymer thin films are considered a homogenous layer of polymer melt formed on a flat surface. Dynamics of such thin films are accessible by optical methods such as light scattering [1], diffuse neutron scattering [2], and mechanical techniques such as AFM [3] , scanning force microscopy [4], tribology [5] etc. Further methods include X-ray and neutron reflectivity [6] [7], dielectric relaxation [8] and many more.

For dynamical investigations, NMR has earned a special place not only due to the obvious advantages such as site-specificity, non-invasiveness but the ability to probe a certain feature by manipulating the spin system. With a clever choice of the method, or by choosing a combinations of methods, one can obtain information about dynamical processes occurring in a particular time range. For instance, with techniques ranging from conventional relaxometry to spectral analysis to diffusometry, processes such as small-scale reorientation motion(in the range of 100's of MHz) or chemical exchange (up to a MHz), or very slow translation motion of chains (a few kHz) can be precisely studied. Although, no question remains about its potential, its application to thin films, particularly to nano-level thin film, is limited due to a simple, but a non-trivial reason: the inherent poor sensitivity of NMR.

Interesting NMR investigations on thin films on flat substrates have been by Zeghal *et al.* [9] and Rivillon *et al.* [10]. Their investigations showed many interesting features regarding the surface-induced chain orientation, segmental ordering and dynamic heterogeneity in these films. The above studies were done on films above 6 nm in thickness but could not be extended to monolayer level films due to the above mentioned problem of sensitivity. Mann *et al.* [11] proposed the idea of using porous hosts serving as substrates for forming thin films, and were successful in demonstrating that several populations coexist even in sub-monolayer thin films, and more importantly that monolayer thin films can be studied using NMR.

The studies cited above and many others address distinct dynamic and structural features of thin films on flat/porous substrates, however relaxation dynamics of these thin films have not been investigated thoroughly. Dynamics information using conventional relaxometry and diffusometry is very efficient in probing motion, but is limited in its range. Especially motional information from a few 100's of kHz to a few 10's of MHz of ^{1}H Larmor frequency

is difficult to obtain using conventional techniques. Fast field cycling (FFC) [12] [13] is the preferred technique in these cases. By being able to switch the relaxation field (B_0), in principle to any field , it enables one to record relaxation times as a function of the applied field, where the relaxation times are strongly correlated to motion at the corresponding frequency of the field.

FFC has been extensively used in the past to study relaxation dynamics of bulk polymers, elastomers, polymer solutions among other systems. The relaxation dispersion, or the spin-lattice relaxation time as a function of frequency, is a reflection of the spectral density function of the system. Hence, the key to understanding the results lies in the effective prediction/modelling of the spectral density function of the system under study. Such spectral density functions for polymers, and their manifestations in the relaxation dispersion have already been described for model polymer systems.

Dynamics of polymer melts, unlike small molecules, differ qualitatively depending on the molecular weight and can be categorized into two regimes based on their molecular weight [14]. Molecules with molecular weight below the *entanglement critical molecular weight*, $M_w < M_c$, do not overlap sufficiently and the topological constraints are unimportant. In order to feel entanglements, the chains must be several monomers long (typically from a few 10's to up to a few 100's). This regime is further categorized depending on whether long-range hydrodynamic interactions are important for the drag on the chains. Rouse [15] modeled the dynamics by considering only the local dissipation due to frictional forces as the chains slide past one another, a situation corresponding to low molecular melts. Zimm [16] devised a model for dynamics in solutions by considering the hydrodynamic interactions that dominate in solutions.

In the regime of high molecular weight $M_w > M_c$, the polymer chains are no longer short, the chain motion is severely restricted by topological constraints, and the chains cannot cross each other. This situation arises in melts as well as in concentrated solutions. Any mathematical model should account for the topological constraints involved. De Gennes [17] proposed the idea of reptating chains in a matrix of fixed constraints, which was later developed by Doi and Edwards [18], which has come to be known as the *tube/reptation model*. The chains are considered to be reptating in a tube made of neighbouring chains. In the *tube/reptation model* or simply the *tube* model, the notion of entanglements in melt was taken into account as fixed constraints. Schweizer [19] proposed a formalism for taking the entanglement effects into account by a generalized Langevin equation applying a so-called memory function formalism.

FFC relaxometry has been successfully used to study polymers melts above and below

the critical molecular weight and demonstrate many features of the above mentioned models. Clearly, the relaxation dynamics of linear polymer melts bear distinct signature of the dynamics as in the frequency dependence of the relaxation time, as predicted by the models. While a low molecular weight polymer follows the Rouse model, a high molecular weight polymer follows Renormalized Rouse formalism. The *tube* model, was not observed in bulk polymer melts, however, only in polymer melts completely confined inside impenetrable porous walls, irrespective of the molecular weight; the solid pore walls are more representative of the fixed constraints as required by the tube model, than the mobile neighbouring chains. A review by Kimmich [20] summarizes most of the studies made in this field.

These studies clearly demonstrate the power of FFC as a relaxometry technique in studying the underlying dynamics of polymer melts chains in different states. In this thesis, the interesting condition of confined polymer melt chains forming a thin film on a surface is undertaken. The aim of the thesis is on the one hand, to demonstrate how field cycling relaxometry can be used successfully to study thin films in the nano-level, and on the other to improve our understanding of dynamics and order of chains in these thin polymer films, in ways that can uniquely be studied by NMR alone. For this purpose, polybutadiene and polydimethyl siloxane thin films formed on a porous substrates are studied using FFC, transverse relaxometry and Double quantum NMR has been used. Porous γ-alumina membranes and porous silica rods were used as adsorbates in the study. The polymers have different degrees of surface interactions with alumina and silica. γ-alumina pores were cylindrical channels of a porous membrane, and the study was conducted on two different pore diameters to see the effect of surface curvature. Additionally to obtain further insight on the surface conformations of sub-monolayer thin films, paramagnetic relaxation agents were used to distinguish between surface and loose chains.

The structure of the thesis is as follows: In chapter 1, a brief introduction to NMR, followed by relaxometry is given. The chapter then proceeds to address the relation between motion and relaxation. In the next chapter, the background of NMR relaxometry is presented. FC relaxometry as well as technical requirements for this technique and for performing experiments are reviewed in chapter 3. The use of FC relaxometry for the study of polymer dynamics is described in chapter 4. In chapter 5 and 6, the results from investigations of thin films of PB and PDMS on alumina and silica surfaces are discussed. Later in chapter 7, the results of investigations of surface conformations of chains in sub-monolayer films is discussed. The summary of the study and the future outlook of the work are painted in the last chapter of this work. Hereby, the author wishes the reader good reading and hopes the reader gains useful knowledge for his/her work.

Chapter 2

Theory

The group of techniques collectively known as *Nuclear Magnetic Resonance (NMR)* has long been one of the most prominent methods for the investigation of structure and dynamics in material science. Techniques ranging from spectroscopy to diffusion have enabled us to selectively study the dynamics in a wide range of time scales, among which NMR relaxometry has played a pivotal role. This chapter deals with the a brief introduction to NMR relaxometry including the relaxation functions, mechanisms and strategies to determine relaxation time based on the system. More detail on the topics covered below including basics of NMR, NMR relaxometry can be found in the books of Ernst [21], Levitt [22], Kimmich [23], Fukushima [24] McBrierty [25] and many others.

2.1 Basics of NMR

2.1.1 Spin energies

Many atomic nuclei have a spin angular momentum, I, and an associated magnetic moment, μ given by the relation

$$\mu = \gamma I \tag{2.1}$$

where γ is the gyromagnetic ratio of the spin. Being a quantum mechanical quantity, I is quantized, hence the orientation of the associated magnetic momentum is also quantized. Another associated quantum number is the magnetic quantum number 'm' that defines the state of the spin. It can take values from $+I$ to -I, thus for a given nucleus, can have $2I$+1 states.

The z component of the angular momentum vector I_z is given by:

$$I_z = m\hbar \tag{2.2}$$

Here $\hbar$=$h/2\pi$, h being the Planck's constant.

When the spins are subjected to an externally applied static magnetic field B_0, they interact with this external field splitting the energy levels that are degenerate at thermal equilibrium. This interaction is called *Zeeman* splitting. The energy of a magnetic moment is then given by:

$$E = -\mu B_0$$
$$E = -m\gamma\hbar B_0 \tag{2.3}$$

As a result, the different spin states that are degenerate in thermal equilibrium have different energies in a non-zero magnetic field. For an I=1/2 spin (e.g. ^{1}H), m can be +1/2 or -1/2, thus their energies differ by :

$$\begin{aligned} \Delta E &= \mid +\frac{1}{2}\gamma\hbar B_0 - (-\frac{1}{2}\gamma\hbar B_0) \mid \\ &= \gamma\hbar B_0 = \hbar\omega_0 \end{aligned} \tag{2.4}$$

where ω_0 is the larmor frequency of the spins that precess around B_0. In this case, for protons, m=1/2 denotes a spin state with orientation parallel to the magnetic field (also denoted 'up', or '$\uparrow$' or α), and m=-1/2 denotes an anti-parallel orientation to the field (denoted 'down' or '$\downarrow$' or 'β').

The population distribution of these spin states are given by the Boltzmann distribution:

$$\frac{N_-}{N_+} = exp\left[\frac{-\gamma\hbar B_0}{k_B T}\right] \tag{2.5}$$

where N_- and N_+ are the population of the components parallel and anti-parallel to the magnetic field B_0 respectively. The net macroscopic magnetization M_z is the sum of all individual magnetic moments associated with the nuclei aligned parallel and antiparallel to the magnetic field.

2.2 Relaxation in NMR

A static B_0 field acting on a spin long enough, brings the spin to equilibrium, which is defined by a state in which the populations follow Boltzmann's distribution and there are no coherences ($M_z = M_{eq}$, the Curie magnetization; $M_x = M_y = 0$). Application of an on-resonant radio frequency (*rf*) field perturbs the equilibrium by changing both the conditions in most cases (however, a population inversion disturbs the equilibrium without creating any coherences). The spins then undergo two different relaxation processes to return to equilibrium. One, called the *spin-lattice* or *longitudinal* relaxation, results in reverting the population of spins to equilibrium by dissipating excess energy to the environment called the *lattice* and hence the name. The time constant for this relaxation process is denoted by T_1. The other process called *spin-spin* or *transverse* relaxation involves the fading out of coherences in the transverse plane due to energy exchange resulting from dipolar coupling with other spins in the system. Both the relaxation processes are closely related to motion,

thereby making relaxometry a very valuable NMR tool to study dynamics.

2.2.1 The Bloch Equations

The spin equilibrium can be perturbed with an *rf* pulse oscillating orthogonal to the static field direction. The response of a spin system to an *rf* field can be conveniently calculated with the Bloch equations [26]. Especially the transformation into a frame rotating with the applied radio frequency, simplifies the expressions and pave the path for a detailed understanding.

Firstly, in the lab frame, Bloch equations in vector form read as:

$$\dot{\mathbf{M}}(t) = \gamma \mathbf{M}(t) \times \ \mathbf{B}(t) - \mathsf{R}(\mathbf{M}(t) - \mathbf{M}_0) \tag{2.6}$$

where $\dot{\mathbf{M}}(t)$ is the first time derivative of the magnetization $\mathbf{M}$. At equilibrium, $\mathbf{M}$=$\mathbf{M}_{eq}$; and R is the relaxation matrix:

$$\mathsf{R} = \begin{pmatrix} 1/T_2 & 0 & 0 \\ 0 & 1/T_2 & 0 \\ 0 & 0 & 1/T_1 \end{pmatrix}$$

Upon irradiation, the external field can be defined as:

$$\mathbf{B}(t) = \mathbf{B}_0 + \mathbf{B}_{rf}(t) \tag{2.7}$$

If the *rf* wave is a linearly oscillating field of the form:

$$\mathbf{B}_{rf}(t) = 2B_1 cos(\omega_{rf} + \phi)\mathbf{e}_x \tag{2.8}$$

then it can be decomposed into two counter-rotating components, of which only the component rotating in the same sense as that of the spins has any significant effect on M_0

$$\mathbf{B}_{rf}(t) = B_1[cos(\omega_{rf} + \phi)\mathbf{e}_x + sin(\omega_{rf} + \phi)\mathbf{e}_y] \tag{2.9}$$

Transformation of the Bloch coefficients $\mathbf{e}_x, \mathbf{e}_y$, and $\mathbf{e}_z$ into a frame rotating with the frequency ω_{rf} gives

$$(\mathbf{e}_x, \mathbf{e}_y, \mathbf{e}_z) = (\mathbf{e}_x^r, \mathbf{e}_y^r, \mathbf{e}_z^r) * \mathbf{T}(t) \tag{2.10}$$

where the transformation matrix $\mathbf{T}$(t) is defined as:

$$\mathbf{T}(\mathrm{t}) = \begin{pmatrix} cos\omega_{rf}t & sin\omega_{rf}t & 0 \\ -sin\omega_{rf}t & cos\omega_{rf}t & 0 \\ 0 & 0 & 1 \end{pmatrix}$$

The magnetization vector in the rotating frame becomes

$$\mathbf{M}^r(t) = \mathbf{T}(t)\mathbf{M}(t) \tag{2.11}$$

and one obtains the following differential equation:

$$\dot{\mathbf{M}}^r(t) = \gamma \mathbf{M}^r(t) \times \ \mathbf{B}^r - \mathbf{R}(\mathbf{M}^r(t) - \mathbf{M}_0) \tag{2.12}$$

where the effective fields $B^r_{x,y,z}$ are

$$\begin{aligned} B^r_x =& B_1 cos\phi \\ B^r_y =& B_1 sin\phi \\ B^r_z =& B_0 + \omega_{rf}/\gamma = -\Omega/\gamma \end{aligned} \tag{2.13}$$

Here Ω is the effective precession frequency

$$\Omega = -\gamma B_0 - \omega_{rf} \tag{2.14}$$

where ω_{rf}=$-\gamma B_{rf}$. Again, the *rf* field is defined by amplitude B_1 and phase ϕ (the excursion from the x-axis towards the y-axis). The Bloch equations in this transformed rotating frame becomes

$$\begin{aligned} \dot{\mathbf{M}}^r_x(t) =& \gamma[M^r_y B^r_z - M^r_z B^r_y] - \frac{M^r_x}{T_2} \\ \dot{\mathbf{M}}^y_x(t) =& \gamma[M^r_z B^r_x - M^r_x B^r_z] - \frac{M^r_y}{T_2} \\ \dot{\mathbf{M}}^r_z(t) =& \gamma[M^r_x B^r_y - M^r_y B^r_x] - \frac{M^r_z - M_0}{T_1} \end{aligned} \tag{2.15}$$

In an actual experiment, the above equations are to be solved to get the various time constants for relaxation.

2.3 Relaxation and Motion

Relaxation occurs in the presence of randomly fluctuating fields at the Larmor frequency of the precessing spins and other frequencies occuring in the BPP formalism [27]. Thermal motion of the spin-bearing nuclei causes these randomly fluctuating local magnetic fields, which cause relaxation. While molecular motion is not the only cause for relaxation, relaxation caused by molecular motion is an efficient tool to study dynamics. In the case of molecular motion causing relaxation, several mechanisms are responsible for the relaxation, and the apparent relaxation time is determined by the most efficient mechanism. Some of the mechanisms that are responsible are briefly discussed below.

T_1 relaxation can be due to several possible mechanisms and can be defined as:

$$\frac{1}{T_1} = \frac{1}{T_1^{dipolar}} + \frac{1}{T_1^{quadrupolar}} + \frac{1}{T_1^{CSA}} + \frac{1}{T_1^{spin\,rotation}} ... \tag{2.16}$$

Dipolar coupling provides an efficient mechanism for relaxation and is most relevant in systems containing protons. For instance, the magnitude and the direction of the dipolar coupling between nuclear spins in the same molecule change as the molecule tumbles, causing fluctuation in the local field exerted by one spin on the other, resulting in relaxation. These stochastic fluctuation of coupling effects can be intermolecular or intramolecular, the strength of which depends on the time scale of motion.

Nuclei with I>1/2 possess an electric quadrupole moment that interact with the electric field gradient generated by the surrounding nuclei. Such coupling effects dominate relaxation, if present. The magnitude of interaction is dependent on the quadrupole moment of the nuclei and the electron field gradient present.

Another significant contribution to relaxation is the chemical shift anisotropy (CSA). In liquids, this is averaged out due to fast motion. However, in solids and soft matters, the CSAs are not completely averaged out. The contribution of this effect to relaxation is however limited in ^{1}H containing molecules, owing to the small chemical shifts of ^{1}H and the usually more efficient dipolar coupling, but becomes important in other nuclei with a strong chemical shift dispersion.

Rotation of molecules can also cause relaxation, for e.g., rotation of methyl groups, however, by a mechanism different in nature. Molecular rotations cause circulation of charges which correspond to an electric current. This current generates local magnetic fields, which may interact with the magnetic moments of the nuclei causing relaxation.

For the spins, the order of efficiency of the different mechanisms is as follows:

Quadrupolar coupling	> Dipolar coupling	> CSA	>	spin rotations

All of the above mechanisms except spin-rotation mechanism, depend on the fact that a molecular reorientation or translational motion modulates the field due to that particular interaction, creating a randomly varying field at the nucleus. These randomly varying fields can be characterized by an autocorrelation function. In the following section, the autocorrelation function and its fourier transform, the spectral density function, are discussed along with its relevance to relaxation.

2.4 Autocorrelation and Spectral density functions

As was just discussed, spin-lattice relaxation is mainly caused by random fluctuations of space dependent spin-interactions, specially dipole couplings of like spins 1/2 in polymers, although, quadrupolar interactions dominate if present. The time scales of these random fluctuations and their influence on relaxation can be characterized by the autocorrelation function of the fluctuations. Suppose the random fluctuating fields b(t) have a *zero* average, but a non-zero magnitude (whose value depends on the fluctuations), i.e., $\langle b(t)\rangle = 0; \langle b^2(t)\rangle \neq 0$ the autocorrelation function G(τ) can be defined as:

$$G(\tau) = \langle b(t)b(t+\tau)\rangle \tag{2.17}$$

The function describes how, for an ensemble average, the values of this local field 'b' at one time t, is correlated with its values after an interval τ, independent of the instants in time over which it is observed. The correlation time $'\tau'$ examines how long it takes for a spin to lose its correlation with the previous orientation in space. The autocorrelation function at τ=0 is by definition equal to the mean square field.

$$G(0) = \langle b^2(t)\rangle \tag{2.18}$$

According to time dependent perturbation theory, the Intensity or the Spectral density function (I(ω)) defines the transition probability per unit time, and is related to the spin-lattice relaxation rates. The intensity function is on the other hand the fourier transform of the autocorrelation function:

$$I(\omega) = \int_{-\infty}^{+\infty} G(\tau) exp(-i\omega\tau) dt = 2\int_{0}^{+\infty} G(\tau) cos(\omega\tau)) \tag{2.19}$$

For isotropic motions, a reduced autocorrelation function can be defined as:

$$\mathbb{G}(\tau) = \frac{\langle b(0).b(\tau)\rangle}{\langle |b^2(0)|\rangle} \tag{2.20}$$

The reduced intensity function is then defined as:

$$\mathbb{I}(\omega) = 2\langle b^2\rangle I(\omega) \tag{2.21}$$

When defining the normalized autocorrelation and intensity functions the isotropic system is also assumed to be *ergodic*. That is, the average of a single spin over a long time or several spins at a single time covers all possible orientations. This also implies, that although the individual fields fluctuate depending on the exact environment and show a wide range of behavioral differences, the *ergodic* approach adopted here, results in the average local field showing some characteristic memory before it changes in magnitude or direction. Thus the correlation function G(τ) will have the general characteristic that it eventually decays to 0. For the purposes of describing spin-lattice relaxation, assuming it decay exponentially, the normalized autocorrelation and its fourier transform, the Intensity function, are given as:

$$\mathbb{G}(\tau) = exp(-(|\tau|/\tau_c)) \tag{2.22}$$

$$\mathbb{I}(\omega) = \frac{2\tau_c}{1+\omega^2\tau_c^2} \tag{2.23}$$

The different relaxation rates (T_1^{-1},T_2^{-1} and $T_{1\rho}^{-1}$) are generally expressed as a sum of individual contributions of the spectral density functions at different frequencies to the concerned relaxation rate. For a dipolar coupled two like spin-1/2 systems, expressions for the spin-lattice relaxation rates in the laboratory and rotating frames, and transverse relaxation rate (assuming an exponential decay of the autocorrelation function) are given by:

$$\frac{1}{T_1} = \frac{3}{10}\mathcal{K}^2[\mathbb{I}(\omega_0) + 4\mathbb{I}(2\omega_0)] \tag{2.24}$$

$$\frac{1}{T_2} = \frac{3}{20}\mathcal{K}^2[3\mathbb{I}(0) + 5\mathbb{I}(\omega_0) + 2\mathbb{I}(2\omega_0)] \tag{2.25}$$

$$\frac{1}{T_{1\rho}} = \frac{3}{20}\mathcal{K}^2[\mathbb{I}(\omega_1) + 5\mathbb{I}(\omega_0) + 2\mathbb{I}(2\omega_0)] \tag{2.26}$$

where the ω_0 is the larmor frequency of the precessing spins, ω_1 is the frequency of the *rf* irradiation, and constant $\mathcal{K}$ is:

$$\mathcal{K} = -\frac{\mu_0}{4\pi}\frac{\hbar\gamma^2}{r^3} \tag{2.27}$$

Here again, γ is the gyromagnetic ratio of the spin, and r is the internuclear distance between the interacting spin-pair. In case of r representing different spin pairs, the different r for each spin pair should be taken into account, and the final equation for $1/\mathrm{T}_1$ carries an ensemble average $< r^{-6} >$ rather than $(r^3)^2$ as above.

The above expressions are known as the BPP formulae [27]. It can be clearly seen that the motivation behind studying relaxation dispersion, i.e. relaxation time as a function of frequency($\mathrm{T}_1(\omega)$) is to get information about the spectral density function and hence the dynamics. This is explained pictorially represented in fig2.1.

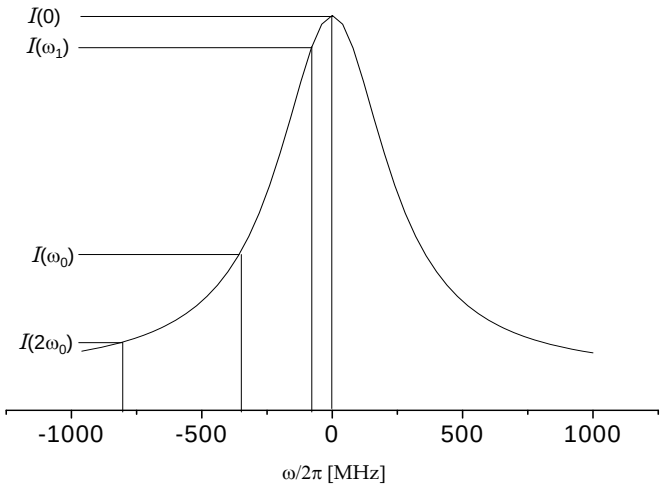

Figure 2.1 : *Spectral density function of a (mono)exponentially decaying process represented by a Lorentzian curve indicating the various components related to the relaxation terms.* ω_0 *and* ω_1 *are the frequency of the probing static magnetic field and the rf irradiation respectively.*

While the above mentioned case of exponentially decaying autocorrelation function is only a model, it is rarely encountered in systems like polymers that are far more complex. The precise form of the spectral density function in such cases is generally very difficult to calculate, however, under certain assumptions can be calculated for complex model scenario. Such functions that have been calculated for certain models of linear polymer melts are discussed later.

2.5 Strategies to determine relaxation time

In order to determine, the longitudinal and transverse relaxation times, T_1 and T_2, several approaches can be adopted depending on the system. Some of the most common approaches and also the ones that were used in this study are outlined in this section. A review of several methods, and a large annotated bibliography of the methods can be seen in [28].

2.5.1 Spin-lattice relaxation

Apart from its importance in reasearch, for most experiments the T_1 basically determines how fast can an experiment be repeated if one needs to have a good signal at the start. Thus it becomes an indispensable parameter to be considered for most NMR experiments. A T_1 relaxation experiment involves tracking the spins coming back to equilibrium conditions from a predefined non-equilibrium established prior to relaxation. In conventional NMR, this can be achieved by either making the population difference between the states to zero i.e., M_z=0 called *saturation* or by inverting the population difference, i.e. $M_z = -M_{eq}$ called *inversion*. This can be done by bringing all the longitudinal (equilibrium) magnetization(M_z^{eq}) into transverse plane with a 90° pulse or by inverting M_z^{eq} into -M_z^{eq} with a 180° pulse respectively. In both the cases, by sampling the magnetization that recovers after a relaxation interval 'τ', the T_1 times can be estimated. The following expressions can be used to estimate T_1 in these cases.

$$M_z(\tau) = M_0(1 - 2exp(-\tau/T_1)) \qquad (Inversion\,recovery) \qquad (2.28)$$

$$M_z(\tau) = M_0(1 - exp(-\tau/T_1)) \qquad (Saturation\,recovery) \qquad (2.29)$$

The advantage of inversion over saturation recovery is that inversion offers a larger dynamic range(-M_z to +M_z), compared to saturation (0 to M_z), hence is more accurate. However, the requirement that an inversion recovery experiment has to begin at -M_z which requires a complete return of magnetization to the static field orientation Z-axis, (i.e M_z=Meq) before every transient consumes time. Saturation can be achieved readily by a train of 90° pulses whose phases are cycled which costs only a few ms at most, where the waiting time between transient is the T_2 of the system. A judicious choice of the method can be made based on the application of the result.

In contrast to conventional NMR methods, in Field Cycling NMR, the spins are allowed to equilibrate to a predefined high field (called the polarization field) B_p where the z-magnetization can be defined as M_z=M(B_p^{eq}). The field is then switched to relaxation field

of interest for a certain relaxation interval τ_r. The resulting magnetization is observed by switching quickly to a high field and applying a read pulse. Thus by observing the magnetization after various relaxation intervals(τ_r), the relaxation time T_1 can be described by the following expression:

$$M_z(\tau_r) = M_0(B_r) + [M_0(B_p) - M_0(B_r)]exp\{-\tau/T_1^{B_r}\} \tag{2.30}$$

This is dealt with in more detail in §4.1.

2.5.2 Spin-spin relaxation

Other than molecular motion, a potential contribution to transverse relaxation (loss of coherences) is the static field inhomogeneities in the sample. In cases where the field inhomogeneities are high compared to the line width due to spin-interactions, the observed decay constant, T_2^* is shorter, and is given as:

$$\frac{1}{T_2^*} = \frac{1}{T_2} + \gamma\Delta B_0 \tag{2.31}$$

$$\tag{2.32}$$

Among the methods used for determining T_2, the most common ones include observing the decay of Hahn-echo(or spin echo), CPMG echo and solid echo. Hahn established [29] a pulse sequence of the form 90° - τ - 90° - τ that resulted in the formation of an echo centered at 2τ resulting from the reversal of the time evolution of the FID. It was also observed that the echo amplitude decreases with increasing τ delay.The echo amplitude M(2τ) for different τ can then be used to extract the T_2 relaxation times using the following equation:

$$M(2\tau) = M_0 exp(-2\tau/T_2) \tag{2.33}$$

When liquids are measured, the high diffusion coefficient should be taken into account in determining the T_2 for such systems. The Carr-Purcell-Meiboom-Gill (CPMG) pulse sequence [30, 31] which consists of a series of 180° pulses instead of just one 180° pulse, applied regularly at a time interval of 2τ results in the formation of an echo in the middle of each pulse separation. The echo amplitude can be analysed with the following expression

to determine T_2:

$$M(2n\tau) = M_0 exp(-2n\tau/T_2) exp(-2/3\gamma^2 g^2 D n\tau^3) \tag{2.34}$$

Where D is the diffusion coefficient, g is the field gradients, γ is the gyromagnetic ratio of the nucleus. By repeating the experiment for different τ, the diffusion coeffiecient can also be computed.

The other basic pulse sequence that is useful for the studies in dipolar solids is the solid echo [32]. The pulse sequence is similar to that of spin-echo except the pulse phases are orthogonal. The sequence is of the form 90°_0 - τ - 90°_{90} - τ, where the subscript denotes the phase in which the pulse is applied. This sequence is effective in refocussing any bilinear terms in the interaction hamiltonian. Direct and indirect dipole couplings terms between two spins appear as bilinear terms in the total spin hamiltonian, therefore this sequence is effective in refocussing such two-spin dipolar couplings. It is of importance in systems such as polymers where more often than not dipolar coupling influences relaxation.

Chapter 3

Field cycling relaxometry and Polymer dynamics

Field cycling has been mainly used to obtain spin lattice relaxation dispersions, i.e. relaxation times as a function of the probing frequency, $T_1(\omega)$. A conventional longitudinal relaxation measurement probes the spectral density of the fluctuations in motion, $J(\omega)$, typically at the Larmor frequency (ω). The spectral densities in turn are the Fourier transforms of the correlation functions G(t). A relaxation dispersion thus provides information about the spectral density function over a broad range of frequencies, which is important to have a comprehensive understanding of soft matter dynamics. Information from this method has been applied successfully in several fields including porous media, liquid crystals, polymers, and many more to learn more about molecular dynamics, order and other intersegmental interaction.

In order to understand the relaxation dispersions, dynamics-specific spectral density function or alternatively autocorrelation function has to be predicted describing the spin interactions. For instance, relaxation dispersions of linear low molecular weight polymers are described by the Rouse model, that takes into account the dynamics of the chain segment in a viscous medium without hydrodynamic backflow or excluded volume effects. Thus a case-dependent model is important to successfully describe the relaxation dispersion.

In this work, FC has been used to probe dynamics of linear polymers confined inside porous substrates. Pertaining to distinct categories of dynamics, three different models have been described. For the case of short linear polymers, that do not form entanglements, Rouse model predictions exist. As the chain forms entanglements, or encounters other obstacles in terms of confinements, their dynamics typically slow down and complicate. For such cases, more complex formalisms such as the Renormalized-Rouse or the Reptation/tube model exists. Interestingly, the relaxation dispersion in such cases shows distinct and clearly distinguishable features.

In this work, the theoretical aspects of field cycling relaxometry and a brief description of the spectral density functions of different scenarios that was briefly mentioned above along with its manifestations in the relaxation dispersions are described. The contents of this chapter are mainly based on the works of R. Kimmich and N. Fatkullin [20, 13].

3.1 Correlation functions for Dipolar and Quadrupolar couplings

The relaxation formalisms of ^{1}H and ^{2}H nuclei are considered in this section although in this work, the relaxation data mainly refers to ^{1}H nuclei. The T_1 relaxation times as measured

from the field cycling technique in this work refers exclusively to proton relaxation from like spins, i.e. the case of homonuclear spins. Although the relaxation mechanism of the two nuclei is different - the mechanism of ^{1}H relaxation is based on fluctuating dipole-dipole coupling of spins while in the case of ^{2}H relaxation, the electric quadrupole moment that the spins possess is subject to quadrupole coupling with local molecular electric field gradients- the relaxation formalisms of the two mechanisms have so much in common that the analytical expressions that it lead to are largely similar. The reason behind this is that the spatial part of the dipolar interaction can be commonly expressed by second-order spherical harmonics $Y_{2,m}(\theta, \phi)$ with m=0, $\pm1, \pm2$ as,

$$
\begin{aligned}
Y_{2,0}(\tau) &= \sqrt{\frac{5}{16\pi}}[3cos^2\theta(\tau) - 1], \\
Y_{2,1}(\tau) &= -\sqrt{\frac{15}{8\pi}}sin\theta(\tau)cos\theta(\tau)exp[i\phi(\tau)], \\
Y_{2,2}(\tau) &= \sqrt{\frac{15}{32\pi}}sin^2\theta(\tau)exp[2i\phi(\tau)].
\end{aligned} \tag{3.1}
$$

Here, $Y_{2,-1}(\tau)=Y^*_{2,1}(\tau)$ and $Y_{2,-2}(\tau)=Y^*_{2,2}(\tau)$ also holds. The only terms in the interaction Hamiltonians relevant for spin-lattice relaxation in homonuclear spin systems (as in this case), in the laboratory frame are those for m=±1 and m=±2 selected by spin operator terms inducing single-quantum and double quantum transitions, respectively. The term m=0 is important only in the case of 'unlike' spins that undergo zero-quantum transitions as a result of energy exchange between Zeeman spin energy states and lattice energy, and in the case of rotating-frame relaxation.

With the spherical harmonics expressed in polar coordinates, the azimuthal and polar angles, $\theta(\tau)$ and $\phi(\tau)$ respectively, describe the instantaneous orientation of the coupling tensor (related to the internuclear vector in the case of dipolar couplings and to the orientation of principal field gradient in the case of quadrupolar interaction) relative to the magnetic field direction B_0. Molecular motions in the sense of reorientations render the relative orientation of the corresponding coupling tensor (dipolar/quadrupolar) time dependent. Consequentially, the dipolar or the quadrupolar Hamiltonians become time dependent and induce spin transitions as predicted by time dependent perturbation theory. In the case of dipolar couplings, the internuclear distance (r) fluctuates as a result of motions, however this is significant only in the case of intermolecular interactions, whereas all intrasegment couplings are associated with constant r values. In fact, the comparison of relaxation behavior of proton and deuteron relaxation, where dipolar and quadrupolar interactions respectively

dominate paves an important way of distinguishing inter and intra molecular contributions to overall relaxation.

In the frame of the Bloch/Wangsness/Redfield (BWR) relaxation theory [33, 23], the fluctuations of the spin Hamiltonians are represented with the aid of normalized autocorrelation functions of the type:

$$\mathbb{G}_m(\tau) = \frac{\left\langle \frac{Y_{2,m}(\theta_0,\phi_0)Y_{2,-m}(\theta_\tau,\phi_\tau)}{r_0^3 r_t^3} \right\rangle}{\left\langle \frac{|Y_{2,m}(\theta_0,\phi_0)|^2}{r_0^6} \right\rangle} \, (dipolar\, coupling)$$

$$\mathbb{G}_m(\tau) = \langle Y_{2,m}(\theta_0,\phi_0)Y_{2,-m}(\theta_\tau,\phi_\tau)\rangle \, (quadrupolar\, coupling) \tag{3.2}$$

The subscripts '0' and 'τ' stand for the instants when the autocorrelations are taken and the brackets for an ensemble average over all spins systems in the sample. As earlier discussed, dipoles fluctuating due to motion induce spin transitions and according to the time dependent perturbation theory, the transition probability per unit time is proportional to the spectral density function or the intensity function of the fluctuating dipole. The spectral density function is in turn the fourier transform of the autocorrelation function:

It should be noted that the spectral density function defined thereby is independent of the 'm' for isotropic systems since it is based on normalized auto-correlation functions (eqn. 3.2).

$$\begin{aligned} I_m(\omega) &= \int_{-\infty}^{\infty} \mathbb{G}_m(\tau) e^{-i\omega\tau} d\tau \\ &= 2\int_0^{\infty} \mathbb{G}_m(\tau) cos\omega\tau d\tau \end{aligned} \tag{3.3}$$

The spin lattice relaxation rate directly reflects the spin transition probabilities per unit time for single and double-quantum transitions and is proportional to a linear combination of spectral densities of the form:

$$\frac{1}{T_1} = C_{coupl}[I(\omega) + I(2\omega)] \tag{3.4}$$

where ω is the resonant Larmor frequency of the nuclei. The analytical form of the above equation is valid for systems of homonuclear dipolar coupled spins.

3.2 The three components of polymer dynamics

The three most popular models describing dynamics of linear polymer melts are the Rouse model [15], the renormalised Rouse model [19] and the tube/reptation model [17, 18]. While the Rouse model describes the dynamics of unentangled polymer melts ($M_w < M_c$) by not considering intermolecular interactions due to entanglements, the other two models consider entangled polymer dynamics ($M_w > M_c$). Whereas in the tube model the entangling (surrounding/confining) chains are modelled as stationary, the renormalized Rouse model assumes the entangling chains as both confining as well as mobile. (As will be seen, this model accounts for the non-observance of reptation characteristics in entangling melts, while the reptation/tube model originally predicted for entangled dynamics predicts the characteristics of polymer melts confined inside hard impenetrable pores).

Polymer dynamics cover a wide range in time scales. However, the shortest time scale describing polymer dynamics is the segment fluctuation time (τ_s) defined as the time constant of motion occurring inside the so-called *Kuhn* segment, which in turn is defined as the shortest segment length above which no orientation correlations with the neighbouring Kuhn segment exists. At the same time, the length of the kuhn segment is large enough to permit the neglect of any stereochemical restriction of the orientation of the Kuhn segments relative to each other. Thereby, the chemical structure, bonding and interactions at the molecular level are neglected and accounted only indirectly by parameters such as friction coefficient η. However far fletched, this assumption of independence of chain dynamics (and other related physical phenomena in the field of polymer dynamics) from the local small-scale details holds true in almost all cases (known as the concept of *universality*).

Based on the times scales of different processes, the polymer dynamics are broadly categorized into three components relevant for NMR relaxometry. The experimental frequency/temperature window accessible by NMR relaxometry is schematically shown along with the three components of polymer dynamics in fig. 3.1 [13].

3.2.1 Component A

Component A comprises of motion at very short length scales. It represents fluctuations occurring within the Kuhn segment up to the time scale $\tau = \tau_s$. In addition, the monomer side group rotations contribute, if such groups exist. All reorientations, corresponding to component A, cover only a solid angle range of the interdipole vector (in case of ^{1}H) or the electric field gradient axis (in case of ^{2}H). A consequence of this restricted motion is that

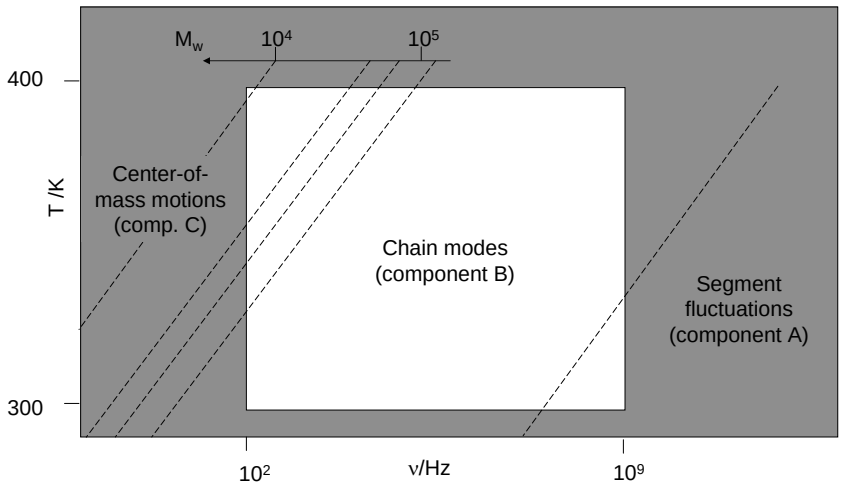

Figure 3.1 : *The experimental window of field cycling relaxometry in combination with high field techniques [13]. As can be seen, FFC predominantly probes the chain mode regime while the other components can be probed only for restricted molecular weights and temperature ranges.*

the correlation functions of dipolar and quadrupolar correlation functions do not completely decay to zero leaving a residual correlation that is decayed further only by chain modes. The correlation function specific for component A can be written as:

$$G_A(t) = g_A(t) + G_A(\infty) \tag{3.5}$$

where $g_A(\tau \gg \tau_s) = 0$. With $G_A(\infty)/G_A(t) = 10^{-3}...10^{-2}$, it can be seen that most of the orientation correlation function decays already due to component A. The slower components B and C can therefore correspond to only a small residual value. This strong correlation decay due to component A consequentially determines the T_1 minima related to the value of τ_s via the minimum condition $\omega\tau_s \approx 1$. The values determined by T_1 minima corroborate that the frequency range of FFC largely corresponds to the time limit $t \gg \tau_s$, i.e. the technique majorly probes the chain mode regime beyond the local segmental fluctuations.

3.2.2 Component B

Chain motions longer than τ_s and shorter than the terminal relaxation time τ_t ($\tau_s \ll t \ll \tau_t$) corresponds to component B. This regime is independent of molecular mass and refers to the hydrodynamic chain mode regime which is of particular interest in the context of chain dynamics models. The spin lattice relaxation dispersions measured by field cycling

relaxometry technique are largely governed by this component.

3.2.3 Component C

Being the cut-off process for component B, this relates to the terminal chain relaxation time τ_t, after which all memory of the initial conformation is lost. This manifests into an 'extreme narrowing' plateau at the low field in the relaxation dispersion. Since this cross-over is connected with τ_t, it is strongly dependent on the molecular mass. This effect therefore shows up in the experimentally accessible frequency window of NMR relaxometry only for relatively low molecular masses.

3.3 Correlation functions on the basis of time scale of motion

A total expression for the correlation function for polymer dynamics relating three partial correlation functions based on the three components can be expressed as:

$$G(t) = G_A(t) * G_B(t) * G_C(t). \tag{3.6}$$

The subscripts denote the partial correlation functions corresponding to the three components. These functions are interpreted as probabilities that the respective fluctuations have not yet taken place at time t. Applying the different time limits for each of the normalized partial correlation functions, i.e.

$$\begin{aligned} g_A(t > \tau_s) &\approx 0 \\ G_B(t \leq \tau_s) &\approx G_B(0) = 1 \\ , G_C(t \leq \tau_t) &\approx G_C(0) = 1 \end{aligned} \tag{3.7}$$

and applying the above relations into eqn.3.6, we have

$$G(t) \approx g_A(t) + G_A(\infty) * G_B(t) * G_C(t) \tag{3.8}$$

where $G_A(\infty)$ is the residual correlation remaining after decay due to component A and is a constant. G_C becomes relevant only for molecular weights close to M_c. For higher M_w ($M_w > M_c$), the fluctuation rates due to component C appear only in the lower frequency end of the relaxation dispersion, in which case $G_C(0) \approx 1$.

In the experimental window of FFC (typically $10^3 < \nu < 10^8$), and for molecular weights

$M_w > M_c$, the most relevant component that is probed is the component B. That is, as was mentioned earlier, the correlation function that corresponds to the relaxation dispersions can be primarily identified with the component B according to:

$$G(\tau_s < \tau < \tau_t) \approx G_A(\infty) * G_C(0) * G_B(t) = const\, G_B(t) \tag{3.9}$$

The component B is also of great interest for testing the model polymer dynamic theories since it describes the chain mode regime. Thus NMR relaxation data from FFC can be directly used to compare predictions of the theories [15, 19, 17, 18].

3.4 Rouse Dynamics for unentangled polymers (M≪ M_c)

The Rouse theory of polymer dynamics applies to low molecular weight polymers with $M_w < M_c$ and dilute solutions where entanglements do not form yet. It considers the dynamics of an isolated Kuhn segment chain in its bead and spring form in a viscous medium without hydrodynamic backflow or excluded volume effects. The effective intramolecular interactions between the segments are approximated by entropic harmonic interactions, reflecting the Gaussian character of the large-scale chain conformation while the intermolecular interactions (with the surrounding viscous medium) are taken into account by friction and stochastic forces acting on the segments. The T_1 relaxation dispersion predicted [34] based on the Rouse theory is:

$$T_1^{-1} \propto \begin{cases} -\tau_s ln(\omega\tau_s) & for \quad \tau_R^{-1} \ll \omega \ll \tau_s^{-1} \\ \omega^0 \tau_s lnN & for \qquad\qquad \omega \ll \tau_R^{-1} \end{cases}$$

Experimental confirmation of these predictions have been observed for different polymers $M < M_c$ including Polydimethylsiloxane [34] [35], Polyethylene [36] etc.

3.5 Dynamics of Entangled polymers (M≫M_c)

As the molecular weight (i.e. the chain length) of the polymer melt increases above the critical value, the neighbouring chains constrain the dynamics of the studied chain, a concept known as *entanglements*. Rouse model is based on single chain dynamics and neglects the effect of entanglements and does not account for the entangled polymer dynamics. Basically

two theories have been successful in explaining the relaxation behavior of chains that experience topological constraints. The tube/reptation model [17, 18] was proposed to explain the effect of entanglements by modelling the dynamics of the studied *tagged* chain moving inside fictitious tubes made of surrounding chains. However, the assumption of the fictitious tube that is static, results in predicting exponents that are not experimentally observed for entangling polymers but rather for polymers confined inside hard pore walls.

The so called *renormalized Rouse* model, a model developed by Kimmich et al. [37, 20] following the suggestion by Schweizer [19] has been able to describe the power law behavior on a time scale $\tau_t > \tau > \tau_s$ indicative of component B, predominantly probed by the Field cycling technique.

Under this condition, the following power laws have been predicted:

$$\mathrm{T}_1 \propto \begin{cases} M_w^0 \omega^{0.5\pm0.05} & (region\,I\ :\ high\,mode - number\,limit) \\ M_w^0 \omega^{0.25\pm0.03} & (region\,II\ :\ low\,mode - number\,limit) \\ M_w^0 \omega^{0.45\pm0.05} & (region\,III\ :\ inter - segment\,interaction\,limit) \end{cases}$$

It should also be clearly mentioned that the renormalised Rouse model is far different from the tube model in several ways including the frequency limits of different processes as well as the exponents observed.

These power laws given above, have all been observed for different polymers at different conditions of temperature due to the limited experimental window thereby making it the most appropriate model thus far for describing entangled polymer dynamics.

The limits I and II, known as the high and low mode number limits, observed in several polymers cannot still be considered as a decisive backup to the theory. These theoretical exponents are slightly affected by the renormalisation ansatz [19] and cannot be tracked back to elementary principles, hence are subject to some ambiguity. However the basic features such as the two experimentally observable limits and predicted crossover between the limits is an important result in explaining the dynamics of unentangled polymer melts.

Fluctuation of internuclear vector of dipoles from different segments occur as a consequence of displacements of the dipole hosting segments by self-diffusion relative to each other. Self-diffusion is a slower process hence these (intersegmental) fluctuations take much longer when compared to the fluctuations of dipolar interactions of dipoles in the same segment. Recently it has been shown that apart from the effect of slow self-diffusion motion, the averaging of several spin-interactions results in a slower fluctuation of the position of the average than that of an individual spins [38]. Consequently, spin-lattice relaxation affected by intermolecular dipolar fluctuation show at much lower frequencies. The region III

(low mode number -long time limit), occurring at low frequencies is dominated by contributions due to such inter-segmental interactions. This can be tested by comparing proton with deuteron spin lattice relaxation dispersion of the same polymer species at low frequencies. Deuteron relaxation is dominated by (intra-segmental) quadrupole coupling with the local electric field gradient, whereas proton relaxation is subject to intra- as well as inter-segmental interactions. Relaxation dispersion studies of protonated and deuterated PB and PEO melts [37] showed that the region III is absent in the deuterated samples due to the absence of intersegmental interactions.

3.6 Dynamics of confined polymers

Polymers confined inside impenetrable pores undergo anisotropic motions along the axis of the pore. De Gennes developed the reptation theory to explain the dynamics of polymers moving between fixed obstacle. Doi and Edwards extended this theory to the theory now known as *tube/reptation* or simply *tube* theory. Reptation behavior has been observed with fast field cycling when polymers are confined in nanoscopic pores [39], when the confinement size is of the same order of the molecular size, namely the gyration radius, R_g. Based on the theory, four different four different characteristic times, viz. the segment fluctuation time τ_s, the entanglement time τ_e, the Rouse relaxation time τ_R, and the tube disengagement time, τ_d were proposed for polymer dynamics. The theory proposes different dependencies of molecular weight and frequency in different regimes. Two of the experimentally observable dependencies are given below [20, 40].

$$T_1 \propto \begin{cases} M^0\omega^{0.75} & for \quad \tau_R^{-1} \ll \omega \ll \tau_e^{-1} \quad (limit\, II_{DE}) \\ M^{-0.5}\omega^{0.5} & for \quad \tau_d^{-1} \ll \omega \ll \tau_R^{-1} \quad (limit\, III_{DE}) \end{cases}$$

Although reptation characteristics have not been observed in larger confinements, motional restrictions were observed even in (non-interacting) micrometer level confinements [41]. In such cases, the effective *tube* (*tube* as defined in the tube/reptation model) is formed by the neighbouring chains, whose low incompressibility restricts lateral motions perpendicular to pore axis, an effect that has come to be known as *corset effect* [39].

Chapter 4

The Fast Field Cycling Relaxometer

The power of NMR spectroscopy to probe motions in soft matter and complex systems is rather well known with its large number of complex techniques developed in the last few decades that have answered several questions and discovered new phenomena. When applied to investigate systems such as polymers, liquid crystals, proteins, etc. where motions span several decades in frequency, information about reorientations, translational diffusion etc., can be studied at both high field as well as low fields. However, there are several processes in these systems such as Rouse modes and back-bone fluctuations in polymers that occur at intermediate frequencies that cannot be probed by conventional relaxometry/spectroscopy, the main drawback arriving from technical difficulties in the intermediate fields and from the weak signal strength. A preferred method in such cases is the NMR field cycling technique which can be used to study the relaxation times as a function of the applied field, arriving at what is known as the NMR dispersion or relaxometry profile, which is a signature of the auto-correlation function of motion. This method can be applied to systems where complex

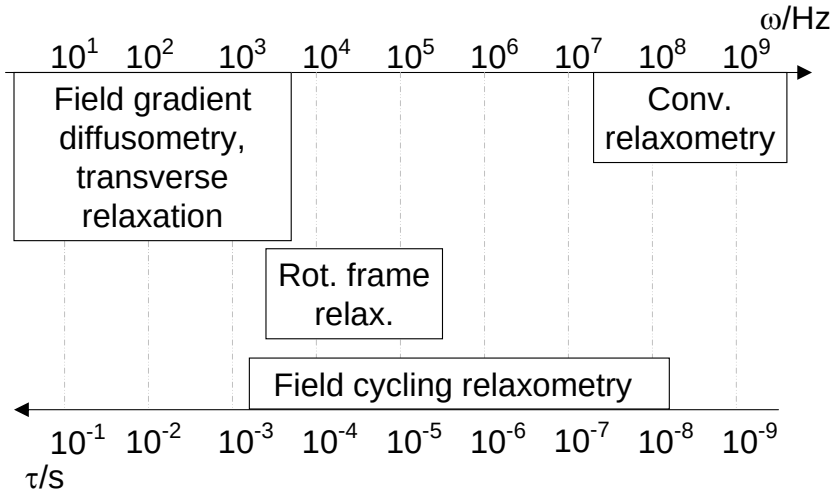

Figure 4.1 : *The time scales(τ) and angular frequency scales(ω) covered by different NMR methods. The ranges indicated refer to proton resonance.*

distributions in motions that span a broad range of time scales exist. The method involves subjecting the sample to a high polarizing field, subsequently subjecting it for a known time to a relaxation field where the relaxation time is to be found, then recording the remaining magnetization at a high field. This cycle is repeated for different durations of the relaxation field to arrive at the relaxation time at that field. A relaxation dispersion can then be arrived at by studying the relaxation times at various relaxation fields. Switching between different fields or cycling the field can be carried out both mechanically as well as electronically. Mechanically, this is done by shuttling the sample between different magnets (fields) using

pneumatic systems. Earliest studies were done this way. However this method involves long switching times and hence is only limited to relaxation times above 100's of ms. For faster field cycling, an electromagnet has been used, where the field is directly cycled without shuttling the sample within a few ms, a method that has come to be known as *Fast field cycling*(FFC). This method enables to record very short relaxation times thus permitting measurements of long scale motions in the order of a few ms. In this chapter the principle of Fast field cycling relaxometry, its technical requirements, and the fabrication details of a modern Fast field cycling relaxometer are discussed.

4.1 General Concepts

The primary and the most widely applied function of a field cycling relaxometer is to measure longitudinal relaxation times (T_1) at various applied fields. In general, commercially available relaxometers employ fields between 1 T to about 10^{-5} T. The general principle of a field cycling relaxometry experiment involves switching the applied field between different values, the magnitude and duration of which is carefully preselected. Depending on the relaxation field at which the relaxation time is to be determined two types of sequences are used. In the case when the relaxation field is low, a sequence involving prepolarizing the spins at high field then switching down to relaxation field and detecting the resultant magnetization at another high field is used. As the relaxation field approaches high values, the polarizing field can be omitted since there is no obvious advantage in pre-polarization of spins as well as a low dynamic range between the polarization and relaxation fields for relaxation. The two schemes are represented in fig. 4.2 [13].

In more detail, for the prepolarizing sequence, the sample is first placed in a high field known as the polarizing field B_p for a time τ_p, in order to pre-polarize the spins before the actual relaxation experiment. In order to ensure maximum polarization, the field B_p is chosen to be high and τ_p is chosen to be at least as long as 5*T_1 of the system under study at B_p. The attained Curie equilibrium magnetization then is $M_0 \propto B_p$. Next, the field is switched from B_p to the preselected relaxation field B_r at a rate fast enough to prevent excessive relaxation losses, yet slow enough to allow for adiabatic field changes (see§4.2.3). Ignoring any relaxation losses during switching, the initial magnetization at the relaxation field $M(0)=M_0(B_p)$ will relax to the new Curie equilibrium magnetization of the relaxation field $M_0(B_r)$ with a relaxation time $T_1^{B_r}$, so that the magnetization evolves according to the

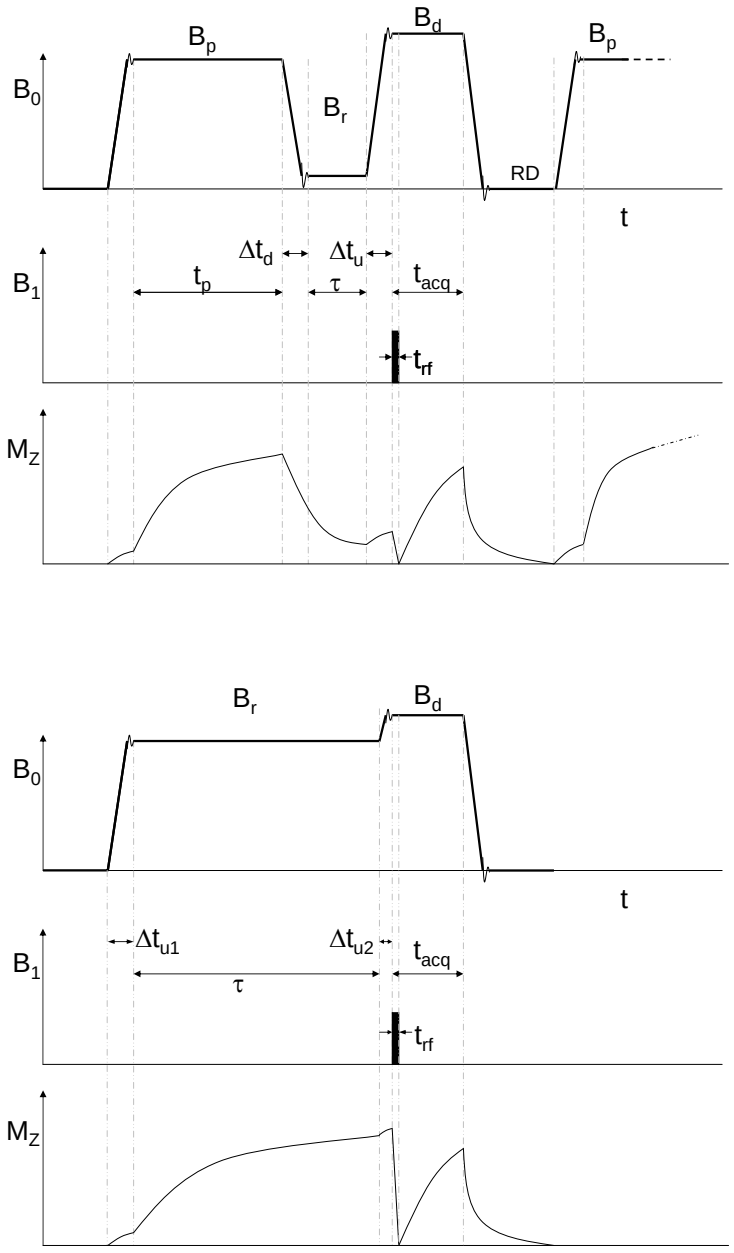

Figure 4.2 : *The two basic field cycling sequences for measuring NMR dispersions. (Top) For cases where $B_r \ll B_p$, a pre-polarization sequence is used, with the application of the polarization field. As the relaxation field increases and approaches polarization field ($B_r \geq B_p$), a non-polarization sequence is applied (Bottom). Shown are the magnetic flux density (B_0), radio frequency amplitude (B_1) and the magnetization (M_z) with the approximate relaxation curves. t_p- polarization time, τ- relaxation interval, $\Delta t_{u/d}$- upward/downward switching time including the settling interval.*

following solution of Bloch's equation:

$$M_z(\tau) \quad = \quad M_0(B_r) + [M_0(B_p) - M_0(B_r)]exp\{-\tau/T_1^{B_r}\} \tag{4.1}$$

The magnetization given above is the remaining magnetization after the relaxation interval τ_r which can be detected with a suitable 90° pulse after switching to a detection field B_d, normally kept high for technical reasons (see§4.2.4). Then the whole experiment is repeated by changing τ_r. In the above, the switching intervals were not considered. Upon consideration of the finite switching intervals (Δt_d) and (Δt_u) for the downward and upward switching respectively, the magnetization at the detection field becomes:

$$M_z(\tau + \Delta\tau_d + \Delta\tau_u) \quad = \quad [(M_z(\Delta t_d) - M_0^r)e^{-\tau/T_1^{B_r}} + M_0^r]e^{-c_1^u} + c_1^u \tag{4.2}$$

where c_1^u and c_2^u are switching constants related to the instantaneous spin-lattice relaxation time. The relaxation behavior to be evaluated is of the form:

$$M_z^{detected}(\tau) \quad = \quad M_z^\infty + \Delta M_z^{eff} e^{-\tau/T_1} \tag{4.3}$$

where M_z^∞, ΔM_z^{eff} and T_1 are fitting parameters. M_z^∞, ΔM_z^{eff} are implicitly defined in the equation 4.2.

The relation shows that the relaxation is a function of $T_1^{B_r}$, and that there are no systematic errors occurring due to relaxation losses during switching intervals and the dynamic range of the measurement is important for the accuracy of the measurement. In the other case, when the relaxation field B_r approaches the polarization field B_p, the dynamic range becomes small for accurate measurements for evaluating $T_1^{B_r}$. Hence it is more favorable to omit the polarizing field where the spins relax to the relaxation field from zero field, or use a negative polarization (prepared with an inversion pulse at the end of the polarization field), where the prepared non-equilibrium is negative before relaxing to the new field. The relaxation curve for evaluation then becomes:

$$M_z^{detected}(\tau) \quad = \quad M_z^\infty - \Delta M_z^{eff} e^{-\tau/T_1} \tag{4.4}$$

Measurements made from fast field cycling relaxometry can be supplemented with measurements made at high frequencies in the order of 100's of MHz with conventional relaxometry.

4.2 General Considerations

In order to perform efficient and accurate field cycling experiments, different requirements have to be met and various factors have to be considered regarding the accuracy of the field, the settling times, the switching rates etc. Some of these will be discussed below.

4.2.1 Contributions to the Magnetic field

At high fields, typically above 10 kHz, the influence of additional fields like stray field, Earth magnetic field, and internal local fields from the sample are negligible. As the relaxation field becomes low, it becomes important to consider the contributions due to additional fields in the surrounding and effectively compensate them. Utilizing compensation coils surrounding the magnet then becomes necessary to reach relaxation fields less than 10^{-4} T (about 4 kHz in ^{1}H frequency). Even smaller fields can be probed in such cases, provided that the field is reached and settled in a short enough time for accurate measurements of relaxation times.

Another important external influence is the field distortion due to increasing temperature of the magnet. During the application of high currents for long periods, the strong current passing through the magnet produces heat which in turn produces a mechanical stress that shifts the magnetic field value during the current pulse. This effect is usually present during the whole passage of the current and becomes more important during high current and long pulses. With a temperature compensation system, this can be compensated by adding a time dependent signal to the current control reference that offsets the field shift. This is especially suitable when dealing with long T_1 relaxation times because of the long duration of the applied magnet current.

4.2.2 Specifications of the field cycle

Whether reaching a low relaxation field from a high polarization field or a high detection field from a low relaxation field, the field switching has to occur such that reaching, settling and stabilizing at the desired field all occur within a time in the order of the relaxation time at the relaxation field with a reasonable accuracy of at least 10%. At the detection field, the accuracy and reproducibility of the field should correspond to the bandwidth of the RF system. For effective measurements, the magnetic flux density needed for magnetic resonance should be reproduced with a relative homogeneity between 10^{-5} and 10^{-4}, which is another limiting factor in the measurements. Such relative field homogeneities are feasible

with special coil design and current density distributions. [42, 43]. Being sufficient for most applications, the switching times for the detection field is defined by the time needed until the final field is stabilzed with an accuracy of between 10^{-5} and 10^{-4}.

4.2.3 The adiabatic condition and the optimal switching rate

The switching rates especially at low field where the relaxation times of most systems are very short, have to be high in order to prevent any relaxation losses during transition. Modern field-cycling relaxometers reach switching rates as high as 1000 T/s ensuring minimal losses during transition between different fields. For effective transfer of magnetization at the end of polarization field to the relaxation field and from the relaxation to the detection field, the the switching time τ_{swt} has to be shorter than the relaxation time at the relaxation field, i.e. the condition $\tau_{swt} < T_1^{B_r}$, has to be met. Longer switching times reduce the signal variation range and hence the experimental accuracy, although systematic errors do not occur due to long switching times (see eqn4.2).

The switching rate can be as high as possible as long as the adiabatic condition [44] is fulfilled. The adiabatic characteristic of a process is when no transitions occur: the spin system always resides in eigenstates of instantaneous Hamiltonian, and the populations at different levels are preserved. This is given by:

$$\frac{1}{B^2}\left|\overrightarrow{B} \times \frac{d\overrightarrow{B}}{d\tau}\right| \quad << \quad \gamma B \tag{4.5}$$

where $\overrightarrow{B} = \overrightarrow{B_0} + B_{loc}$ is the total flux density felt by the nuclei. B_{loc} is the local field caused by secular spin interactions. That is, the local magnetization should always remain aligned along the quantizing field $\overrightarrow{B}$: the directions of the local fields are more or less randomly distributed and do not coincide with that of the external magnetic flux density $\overrightarrow{B_0}$. At high external flux densities, B>>B_{loc} the local fields can be neglected and the quantization direction coincides with the direction of $\overrightarrow{B_0}$. Under such conditions, there is no upper limit of the field variation rate. It remains always adiabatic. In essence, the switching times must be shorter compared to the relaxation times, but longer compared to the Larmor frequency.

4.2.4 Signal-to-Noise ratio

Signal-to-noise ratio is one of the crucial limitations of this technique. Like in conventional NMR spectrometers, for signal accumulation with phase sensitive detection, the detection

field has to be reproduced accurately enough in subsequent transients. However averaging may be restricted due to the intrinsic limited stability of the field cycling systems.

The single-transient signal-noise ratio [33] can be written as:

$$S/N \quad \propto \quad B_0 \xi \sqrt{\frac{\eta Q V_s}{k_B T} \left(\frac{\nu_0}{\Delta\nu}\right)}, \tag{4.6}$$

where η is the filling factor of the coil, Q is the quality factor of the coil, V_s is the sample volume, k_B is the Boltzmann constant, T is the absolute temperature, ν_0 is the Larmor frequency, $\Delta\nu$ is the bandwidth of the receiving filter and amplification system, and $\epsilon<1$ represents the reciprocal noise level of the receiver electronics. It can be seen that the S/N ratio increases with $B_0^{\frac{3}{2}}$, while the use of high polarization and detection flux densities, large samples, high Q coils, low-noise receivers and narrow RF filters also help increase the S/N ratio.

Since in the case of field cycling relaxometry, the polarization field and the detection field are different, the eqn. 4.6 has to be modified as:

$$S/N \quad \propto \quad B_p \xi \sqrt{\frac{\eta Q V_s}{k_B T} \left(\frac{\nu_d}{\Delta\nu}\right)}, \tag{4.7}$$

where B_P is the polarization flux density, and ν_d is the Larmor frequency of the detection field related to the flux density at that field (B_d) by $\nu_d = \gamma B_d/2\pi$. Thus it is advantageous to use high polarization and detection fields. However, long periods of polarizations (typically $5{*}T_1^{B_p}$) at high field induces thermal stresses on the magnet due to Joule heating which leads to other difficulties (see §4.2.1), therefore practically it is favorable to use a moderate polarization field.

4.3 Hardware concepts

The earliest form of field cycling relaxometry involved shuttling the sample between different static magnetic fields (see [45, 46] and several references in [12]). Due to the finite time involved (in the order of 100's of ms) in mechanically shuttling the sample, this methodology was limited to measuring only longer relaxation times. The first electronically switched field-cycling instruments facilitating measurements of relaxation times smaller than 100 ms were built in the 60's by Redfield and co-workers at the IBM Watson Research Laboratory [47] and by Kimmich and Noack at the University of Stuttgart [48]. Since then numerous developments have been made in this field. Currently, the Stelar FFC 2000 spectrometer,

commercially manufactured by Stelar S.r.l. has been widely accepted among research groups interested in Field cycling relaxometry.

The fig. 4.3 shows the general architecture of a typical modern field cycling relaxometer (the architecture is based on the Stelar FFC 2000 relaxometer). The core components of the field cycling relaxometer includes the magnet with an efficient design that is compact for efficient cooling but with a large enough bore for the desired sample size and good field homogeneity, a switchable power supply so that the field reaches desired power in a short time and maintains stability once reached, and an efficient cooling system that maintains the magnet temperature inside a permissible limit. Other important components includes the spectrometer and the temperature control unit among other things. In this work, the relaxometer manufactured by Stelar S.r.l has been used for investigations. The following discussion is focussed on components used in one such relaxometer although other models, materials and approaches also exist. For a latest review on field cycling, see [13].

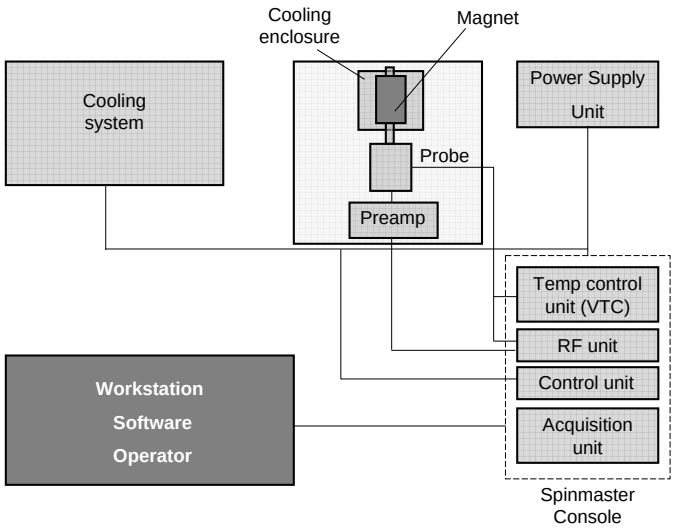

Figure 4.3 : *Architecture of a modern fast field cycling relaxometer based on the model of Stelar FFC 2000 [13].*

4.3.1 The Magnet

A prime requirement of a field cycling magnet is that the energy stored in the magnet is cycled in and out fast and the associated field remain homogenous in the order of 10^{-5} relatively in the region of the sample to have magnetic resonance phenomena during detection as discussed in §4.2.2. An additional requirement of the magnet is that it should withstand the strong mechanical impulses during field switching. Considering the above requirements along

with the cost and efficiency, the optimum design involves a two-layered air-core magnet. In Stelar FFC 2000 equipment, a silver air-core magnet is employed providing a maximum field of upto 1 T and a homogeneity of 200 ppm over a volume of 1 cm^3.

4.3.2 The Power supply

The magnet power supply facilitating fast switching, fast settling and high relative stability makes it the second most important unit in the system. The crucial element of this set up is the switching between the high and low current states. In a typical cycle, currents of several hundred Amperes and peak voltages of several kV are encountered. For this purpose electronic switches involving semi-conductor devices such as metal oxide semiconductor field effect transistors (MOSFETs), gate turn-off (GTO) thyristors, and insulated gate bipolar transistors (IGBTs) are used. In Stelar FFC-2000, the fast switching is facilitated by a collective set of MOSFETs arranged in parallel. Although MOSFETs are sensitive to over-charges when parallel arrangements deviate from symmetry, this arrangement allows the reliable completion of the experiment even when a few MOSFETs are broken. Yet, IGBTs combining the advantages of Bipolar transistors and MOSFETs are considered the most favorable switches for field cycling purposes.

4.3.3 The cooling system

High currents induces high mechanical and thermal strains on the magnet which in turn distort and shift the desired set field. While such aspects are taken care of partially during the designing stage of the magnet, an efficient cooling system to dissipate the Joule heating produced during passage of high currents is paramount to reduce these strains. While liquid nitrogen as a cooling agent is ideal for several reasons, handling inconveniences and costs due to high consumption prevent it from being used for practical purposes unlike in high field. As a consequence, the field-cycling relaxometers currently in use are non-cryogenic systems.

The use of water, which is most economic, is unfavorable because of its electrolytic properties, hence low-viscosity oils such as liquid freon or perfluoroheptane (PFPE) are the most favoured solution. As a primary coolant in Stelar FFC 2000, commercially available PFPE (Galden D80 from Ausimont) known to be chemically inert with a high thermal capacity is used. Using flourinated liquid allows to prevent any 'spurious' proton signal from the coolant present all around the magnet during measurements. This primary coolant runs in a closed loop which is further cooled by a secondary cold water circuit thereby maintaining

Galden at an optimal temperature of 14-16 °C. Further cooling is avoided to prevent water vapour condensation problems.

4.3.4 The temperature controller for the sample

It is well known that the relaxation times depend strongly on the sample temperature, hence it becomes paramount to control the temperature and maintain it constant during the measurement. Temperature dependent measurements also give additional information about the system like during transitions. Because of the limited space available and other reasons, generally the temperature control system incorporates flowing air preheated to the desired temperature. This also reduces unnecessary design considerations if the sample volume is unobstructed.

In Stelar FFC 2000 equipment, the temperature is controlled by a standard gas-flow system. This is monitored by the VTC or the Variable temperature unit using a feedback control mechanism with input from a thermocouple mounted in the pathway of the air. The temperature range specified by the manufacturer is from -100°C upto + 100 °C with a precision of 0.1 °C restricted by the probe. While dry air, heated prior to entering the sample volume is used during high temperature measurements, cold nitrogen gas is used for low temperature measurements.

4.3.5 The NMR console

The NMR console is the heart of the Field cycling relaxometer and incorporates various systems for the functioning and monitoring of measurements. It includes the radio frequency unit, the pulse programmer and the signal acquisition unit, and specific to Stelar FFC 2000 (known by the commercial name *Spinmaster Console*, the variable temperature unit described in the earlier section (see §4.3.4). The RF broadband unit of the Spinmaster console of the Stelar FFC 2000, operates in the range from 2.5 MHz to 80 MHz allowing to investigate different nuclei and is equipped with a two channel receiver with quadrature detection.

Chapter 5

Experimental methods

5.1 Materials and Equipment

Polybutadiene (PB) and Poly(dimethylsiloxane) (PDMS) melts were used in the study as purchased from Polymer Standards Service GmbH, Mainz, Germany. As confining substrates, porous alumina membrane discs were obtained from Whatman Int'l ltd., UK, and porous silica rods were obtained from Corning Ltd. were used. The solvents chloroform and toluene were obtained from Fischer scientific and used without further distillation.

For PDMS, melts with molecular weights 200200, 33300 and 10300 g/mol were used (denoted PDMS200k, PDMS30k and PDMS10k respectively). With the critical molecular weight for PDMS being M_c=25000 g/mol [49, 50],the molecular weights of the melts lie below (PDMS10k), above (PDMS30k) and well above (PDMS200k) the M_c respectively. The polydispersity indices for all of the samples were less than 1.1 as specified by the manufacturer.

For PB, a melt with molecular weight 2020 g/mol (denoted as PB2k) was used. The polydispersity index for the melt was 1.01. With the critical molecular weight (about 4000 g/mol [49])of PB, the melt lies below M_c and hence molecules do not form entanglements.

Porous membranes of γ-alumina, commercially known as Anopore^{TM}, available as discs of 60 μm thickness and variable disc diameter were used. The pores are regular cylindrical channels of diameter 20 nm and 200 nm (A20 and A200 resp.) running parallel through the thickness of the membrane disc. However recent studies show that the pore structure is complex, and the membranes may possess asymmetric as well as multiple pores [51]. The porosity of the discs is between 25-50% as specified by the manufacturer.

Commercially available porous silica rods , Vycor®(glass no:7930), has a composition of 96% SiO_2, about 3-4 % the B_2O_3 and less than 1% of oxides of Na, Al and Zr . The nominal pore size is 4 nm (96% of the pores are 4$\pm$0.6 nm) and porosity 28% as specified by the manufacturer. The specific surface area is 250 m^2/g, and the apparent dry density is 1500 kg/m^3. The solvents used for preparing polymer solutions viz. toluene, and chloroform were at least 99% pure and were used without further distillation.

Field cycling measurements were all carried out with a commercial Stelar FFC-2000 1T relaxometer from Stelar s.r.l., Mede, Italy in the range from 10 kHz to 25 MHz. Transverse relaxation and DQ measurements were made at high field 4.7 T superconducting magnet supported by a Bruker DSX-200 spectrometer.

5.2 Methods

In the following section, the preparation of the polymer melt thin films in porous anopore membranes and in vycor is described along with the sample characterization. Then the experimental technique and methodology used for performing the field cycling experiments, the transverse transverse relaxation measurements and the double quantum measurements are discussed.

5.2.1 Preparation of Polymer thin films in porous Alumina

To prepare thin films of polymers (PS and PDMS), solvent evaporation technique was adopted. For PDMS, chloroform was used as the solvent and for PB, toluene was used, both being good solvents for the respective polymers. The polymer melt was dissolved in their respective solvents and was used at least after 6 hours of preparation. Prior to this, the Anopore membranes were rinsed in chloroform and then ultrasonicated in a new batch of solvent for 5 minutes. This was followed by air-drying for about 5 minutes and then evaporating the traces of solvent in high vacuum at elevated temperatures (100-110 °C) for about 12 hours. The high temperature and vacuum ensures any small traces of solvent and most of the moisture to be removed before the pore surfaces are coated with polymer. The clean membranes were then immersed in the polymer solution for about 5-15 mins. This last step was carried out in an inert atmosphere of argon in order to avoid contact with air. The weight increase for longer periods of adsorption was negligible, as has been observed by other authors [11, 52]. Thus the polymer adsorption reaches equilibrium in this short duration due to the low viscosity and high mobility of chains in solution.

After the adsorption process, the membrane discs are removed, and evacuated overnight at 50-60 ° C to the solvent. From the difference in weights before and after adsorption, the amount of polymer adsorbed can be determined. The total deposited polymer weight can be controlled by varying the concentration of the solution. For the study, each membrane contained typically between 0.5 mg and 6 mg. To increase the signal-to-noise ratio, up to 4 membranes were used in some samples. Although the unloaded weight of each membrane slightly varied, the weight differences arise from the dimensions of the membranes, and the pore wall thickness and also from the weight differences in the polypropylene ring that supports the membrane.

For the calculation of layer thickness the following conditions were assumed. (i) the amount of polymer is a constant inside each individual pore; (ii) the polymer forms layer

whose thickness is uniform inside each pore; and (iii) any layer thickness or molecular weight dependence of the density of the layer is neglected. The above approach serves well the estimation of the layer thickness, however by no means it is argued that this represents the real physical dimensions in the pore matrix.

Using these assumptions, in a pore of diameter $2R$ and height H, the polymer forms a film of thickness t_P. X is defined as the ratio between the volume of the polymer film to the volume of the pores in the membranes. i.e.

$$\begin{aligned} X &= \frac{V_{PDMS}}{V_{pores}} \\ &= \frac{W_{PDMS}/\rho_{PDMS}}{V^{bulk}_{Alumina} - (W_{mem}/\rho_{Al_2O_3})} , \end{aligned}$$

where W_{PDMS} and W_{mem} are the weight of the polymer and the dry membrane, respectively, and $V^{bulk}_{Alumina}$ corresponds to the volume of a solid alumina disk of the same dimensions as the membrane.

X can also be expressed by the ratios of cross-section areas

$$\begin{aligned} X &= \frac{A_{poly} \cdot H}{A_{pores} \cdot H} \\ X &= \left(\frac{R^2 - (R - t_P)^2}{R^2} \right) . \end{aligned}$$

Simplifying, one derives

$$t_P = R \cdot (1 - \sqrt{(1 - X)}) .$$

As seen t_p represents a consistent way to characterize the samples, however this estimate is not claimed to be a physical quantity of the thickness of the layer. The average nominal thicknesses are arrived at from the densities of the polymer and alumina from literature.

5.2.2 Preparation of partially filled Porous Silica

Vycor tends to adsorb organic vapors from the atmosphere. In order to remove such impurities following the recommendations of the manufacturer, the samples were boiled in 30% H_2O_2 for 30 min and subsequently dried in high vacuum at about 110 °C. Normally, such clean rods look transparent and is an indication of purity.

The cleaned rods were submerged into the polymer solution for at least up to 24 hours with minimal exposure to air. After removal of the rods from the solution, the outside of the rods were wiped clean to remove polymer from the outer surface and subsequently, the rods were taken to the vacuum chamber and evacuated at high vacuum at 50 °C for about 8 hours.The level of polymer saturation in the pores was controlled by varying the concentration of the polymer solution.The evacuated samples were then sealed in glass tubes.

5.2.3 Fast field cycling relaxation measurements

Frequency dependent longitudinal relaxation times $T_1(\omega)$ were recorded in the range of ^{1}H Larmor frequencies between 10 kHz and 25 MHz in typically 23 equally spaced logarithmic steps. Although data at even lower frequencies can technically be recorded, since the equipment did not include external coils for compensation of Earth and stray field contributions, the low field measurements were generally not performed or not included. For polarizing the spins, specially for measurements at low field, a field of 0.45 T (corresponding to a frequency of 20 MHz) was used. A threshold frequency of 9 MHz was set, above which no polarization field was applied prior to relaxation field. The switching rate between the different fields was set at 11 MHz/ms. The field settling time , that is the time allowed for the field to switch from one value to the other and stabilize at that value was set to 2.3 ms. For the measurements, up to 48 accumulations were acquired for each signal to increase the signal to noise ratio and 20 values of the delay time at the relaxation field were used. No deviation from an exponential relaxation behavior was observed, but owing to the low amount of polymer in some samples, the fitting error - assuming a mono-exponential function - was as high as 8% for the smallest amounts of polymers; individual measurements with larger fitting errors were discarded. The temperature of the measurements was controlled with a variable temperature control unit from the same manufacturers. The temperature was controlled within a deviation of ± 0.1 K from the set temperature.

5.2.4 Transverse relaxation measurements

All Transverse relaxation measurements in this work were done at 200 MHz using a 4.7 T superconduction magnet supported by a Bruker DSX spectrometer. The samples were loaded onto a 5 mm sample tube and measured on a 7mm high-power solid state probe. A 90° pulse length was 2.7 ms long.

For accessing mobile uncoupled spin fractions in the sample, a Carr-Purcell-Meiboom-Gill pulse sequence ($\pi/2^{(\phi)} - \tau - [\pi^{(\phi\pm90^\circ)} - \tau - acq - \tau]_n$) was used. The pulse spacing ($2^*\tau$) was kept to 2 ms with n (number of echoes) up to 2048. The envelope of every even echo was then fitted with a bi-exponential function. Therefore, the observable limits of transverse relaxation become a few ms and 2 s, respectively.

To obtain information about rigid coupled spins which have relaxation times far shorter than probed by CPMG, solid echo pulse sequence was used. Phenomenologically, solid echo perfectly refocusses spin-1/2 nuclei that interact in pairs, while higher order interactions are only partially refocussed [53]. The solid echo experiment ($\pi/2^{(\phi)} - \tau - \pi/2^{(\phi\pm90^\circ)} - \tau - acq$) was performed by varying the delay 'τ' in the range between 2.5 μs to 1 ms between the pulses. The second half of the echo was recorded and the integral intensity was used for analysis.

5.2.5 Double Quantum NMR

Dipolar couplings are averaged out in liquids due to fast isotropic motions. However, in solids and other motionally hindered systems, anisotropy and slowing down of motions render the dipolar couplings to be only partially averaged. The residual dipolar coupling carry valuable information about order and dynamics and is a very useful tool for investigation. One of the common methods to investigate the strength of the dipolar coupling constant is to measure double quantum build-up curves [54], where the build-up depends on the strength of the coupling and the orientation of the spin pairs with respect to the applied static field. In case of a powder sample, information about the strength of coupling which is directly related to the mobility can be accessed.

In this study, an eight-pulse sequence was used to excite double quantum coherences [55, 56] with an appropriate phase cycling. The basic scheme consists of exciting DQ coherences, letting them evolve over the proton spin pairs in the sample, then reconverting them to single quantum coherences to be detected at the end. The pulse sequence used in this study is shown in fig.5.1. Here, however, in the middle of each period, a 180° pulse is applied to refocus any inhomogeneities as well as chemical shift evolution and other linear interactions, and the DQ coherences are reconverted to z-polarization which are detected with a read pulse after a short "z-filter". The DQ build-up curve is obtained by plotting the intensity of the DQ-filtered signal normalized with the single quantum signal intensity as a function of the square of the excitation/reconversion time (τ).

For identical spin pairs, the build-up is a known function of the coupling strength ω_d,

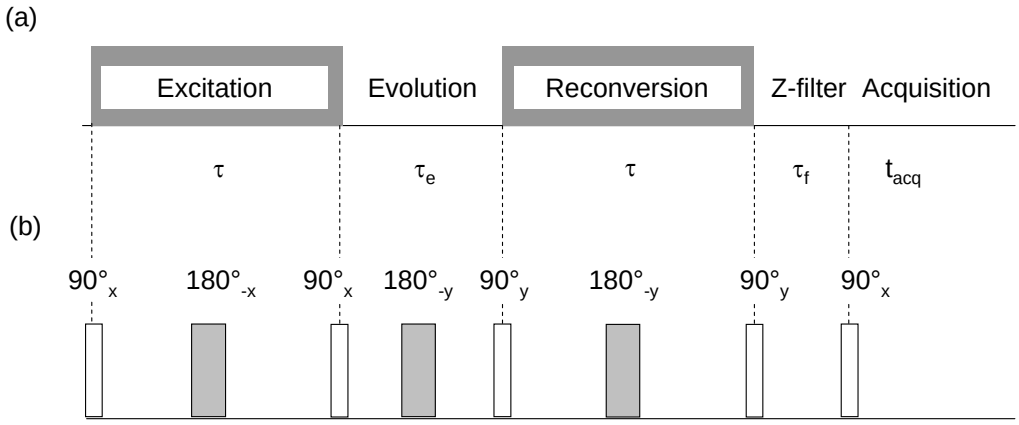

Figure 5.1 : *(a)General scheme for the excitation of multiple quantum coherences. (b)The pulse sequence used in the study to excite double quantum coherences. The excitation/reconversion, evolution , z-filter and detection periods are denoted by* τ*,* τ_e*,* τ_f *and* t_{acq} *respectively.*

expressed in frequency units. In the presence of more than one non-identical spin-pair, the coupling strength can still be expressed in terms of an average parameter, ϖ_d which can be estimated from the initial slope of the build-up curve according to:

$$S_{DQ}(\tau) = \varpi_d^2 \tau^2 \tag{5.1}$$

where $S_{DQ}(\tau)$ is the DQ signal intensity for an excitation time of τ.

Chapter 6

Dynamics of Polybutadiene thin films in porous hosts using field cycling relaxometry

Introduction

Understanding dynamics of polymers in confined state is important since in many applications they exist in confined non-bulk states. From the research point of view, the crossover from bulk to confined state (conditions under which a particular property begins to deviate appreciably from bulk) is important to understand in order to predict the performance and enhance the applicability of the polymer.

Field cycling (FC-NMR) investigations of polymer melts dynamics show characteristic signatures of different models, depending on the molecular weight of the polymer. Polymers with molecular weight below the entanglement critical molecular weight follow Rouse dynamics (§3.4) and those above follow Renormalized Rouse formulation (§3.5). Non-bulk states such as confinements on the other hand, induce deviations in dynamics from the bulk; for instance, when polymers are confined in impenetrable nanoscopic pores, the size of which approaches the molecular size, the dynamics are observed to follow the tube/reptation model(§3.6). The observation of deviation from bulk dynamics even in confinements that are in the μm range [41] is due to the so called *corset effect* [39]. This effect suggests that the confining tube, as defined in the tube model is formed by the neighbouring chains, whose low incompressibility restricts lateral motions perpendicular to the pore axis.

In this work, linear polybutadiene melt has been studied using FC-NMR in bulk and in confined state. Earlier PB investigations with FC-NMR have focussed on melts [57] [37], PB elastomers and copolymers [58]. Studies on melt have clearly shown that PB follows Rouse and renormalized Rouse depending on molecular weight, as predicted. FC-NMR studies on motionally restricted PB due to cross-linking, filler-addition, copolymerization, uniaxial deformation [58], have shown slowing down of motion and additionally in the latter two cases, a change in the motional statistics that can be traced back to a different time dependence of the autocorrelation of segmental orientations. Although several other studies exist on PB copolymers and elastomers especially, not much has been investigated about confined PB systems although such studies exist for several other polymers [41, 59, 60, 39]. Here, PB thin films formed inside porous media of different sizes are investigated; the partial saturation leading to the formation of thin films on the pore walls. Thereby this study aims at throwing light on dynamics of PB thin films formed layers inside confined pores.

To this effect, Polybutadiene was partially loaded in two types of pores differing in size and surface interactions. Porous alumina with high surface/volume ratio with pore size 20 nm and 200 nm, and porous silica(96%) with pore dimension approaching the bulk radius of gyration of the polymer was used. While both substrates are hydrophilic in nature, silica

is known to have a high density of surface hydroxyl groups participating in adsorption [61].

In porous alumina, the size of the pore, hence the surface curvature is expected to play a role. As the pore curvature increases (or as the pore size decreases), the low energy of cohesion of the melt may discourage the spreading of the melt resulting in the formation of non-uniformly spread bulk-like regions. As the layer thickness of the films approaches molecular dimensions, size effects may become relevant for the observed dynamics. Additionally the presence of free air-polymer interface will enhance mobility. In porous silica, the confinement size which is of the same order as the polymer radius of gyration, will induce strong restrictions as has already been shown [62, 63]. The partial filling of the matrix may induce additional degrees of freedom owing to the free air-polymer interface inside the pores, however motions transversal to the pore axis are still hindered.

6.1 Experimental

Polybutadiene melt (M_w=2020 g/mol; PDI:1.07, denoted PB2k) films of varying thicknesses were prepared inside porous Anopore membranes as explained in §5.2.1. The molecular weight of the PB melt used in the study is less than the critical molecular weight of about 2000 g/mol [64, 65]. The bulk radius of gyration (R_g) for this molecular weight is 2.2 nm [66]. The specifications of the various samples are given below in table 8.1.

Table 6.1 : *Polybutadiene thin films in alumina pores*

Pore specification	polymer loading[mg]	Nominal layer thickness [nm]
A200	8.0	6.81
A200	1.7	1.80
A20	10.0	1.05
A20	1.77	0.18

Table 6.2 : *Polybutadiene melt in partially filled porous silica*

Sample	solution conc. [mg/ml]	polymer loading [mg]
V1	40	2.4
V2	20	1.5
V3	10	1.2

6.2 Results and Discussion

6.2.1 PB thin films in large Alumina pores

The relaxation dispersion of PB2k bulk polymer is shown in figure 6.1 along with a master curve constructed by shifting the data relative to a reference temperature(296 K) to view the whole spectrum as is commonly done in other broadband spectroscopic techniques like Dielectric spectroscopy. The validity of the concept arrives from the direct dependence of relaxation rates on the spectral density functions as has been demonstrated earlier [67], barring any change in the shape of the spectral density function, for e.g., during phase transitions. The shape of the master curve corresponds to Rouse behavior as expected for melts with molecular weight less than the critical molecular weight [15, 20] with a logarithmic dependence at high frequencies and tending towards a plateau towards lower frequency.

Figure 6.2 shows the relaxation dispersion of PB2k thin films in A20 and A200 along with the bulk melt at 298 K. The nominal layer thickness of the films investigated here approach monolayer thicknesses while the thickest films are only a few monolayers in size, assuming uniform thickness of the film. If the above assumption was true, a deviation from 3D bulk state should be observed at least for films that have sub-monolayer dimensions.

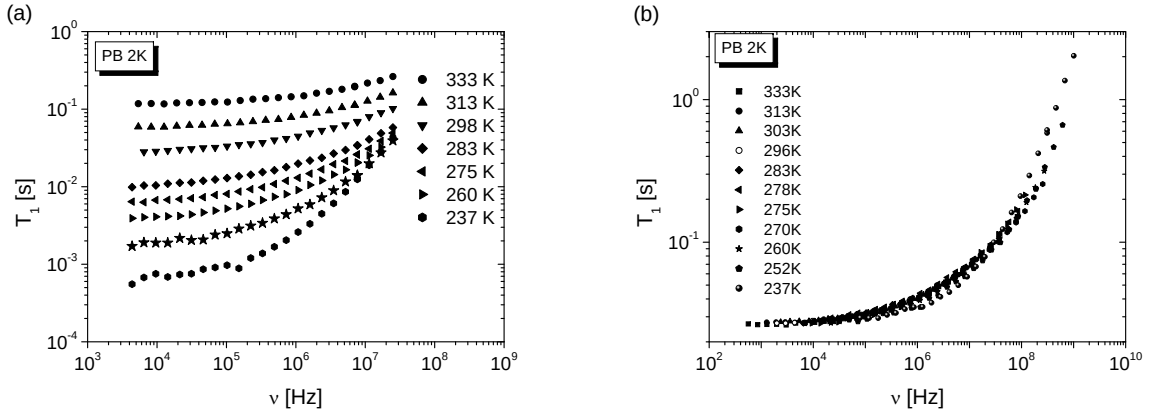

Figure 6.1 : *(a)Relaxation dispersion of a polybutadiene melt(PB2k) at different temperatures. (b)A master curve constructed by shifting individual measurements with reference to 296 K. The master curve demonstrates the features of the Rouse model.(see section3.4.)*

The relaxation dispersion of the thin films in porous alumina show several distinct features: the shape of the relaxation curve is similar to that of the bulk; the relaxation times are close to the bulk at high frequencies and reduced at lower frequencies; the reduction in

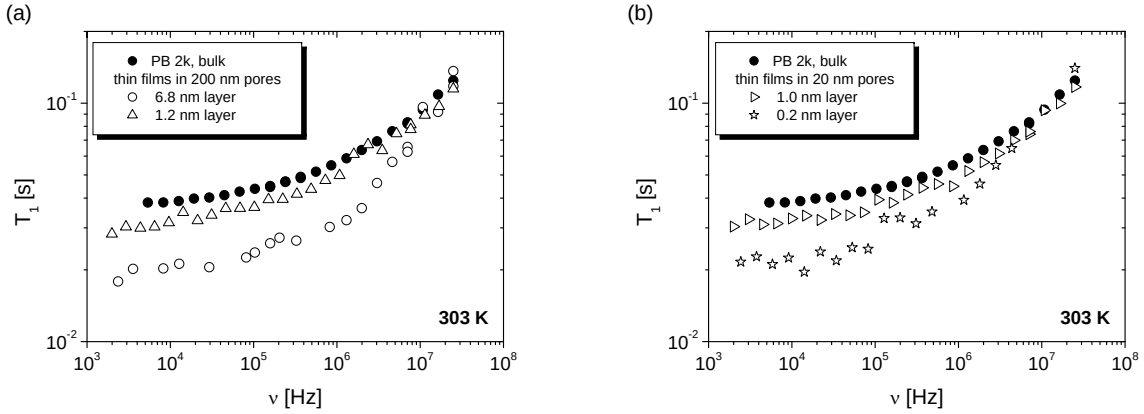

Figure 6.2 : *Relaxation dispersion of PB2k thin films in (a)20 nm pores and in (b)200 nm pores at 303 K. The relaxation dispersion of the melt is also given.*

T_1 at low frequencies is dependent on the layer thickness of the film inside pores of the same size (20 nm and 200 nm); thinner films inside smaller pores show comparatively smaller reduction in T_1 compared to films in larger pores.

The shape of the relaxation curve is qualitatively similar to that of the bulk [15]. This is an indication of the dynamics in these thin films being similar to that in the bulk. For instance, completely confined polymers amongst fixed barriers have been known to show a stronger dispersion [63] as per the predictions of the tube theory [18]. The mobility induced by the air-polymer interface in the case of the films in this study is a clear violation of the conditions required for the observation for reptation [17].

The short scale segmental reorientation motion probed at high frequencies in the MHz region are only slightly affected, if at all, as seen from the converging T_1 values at higher frequencies(>10 MHz). These motions appear to be still fast enough in the confinements similar to the bulk to be motionally averaged. It is the chain modes represented by the reduced relaxation times at lower frequencies that show motional restrictions experienced by motion in times scales of μs, typically corresponding to Rouse modes and eventually translational diffusion at even longer times.

The relaxation dispersion of the films (fig.6.2) shows a trend of decreasing relaxation times with decreasing layer thickness, or in other words, increasing motional restriction (within A200 or A20) due to the effect of the decreasing finite size of the molecular layer. Progressively increasing restriction of lateral motions with thinner layers, specially in the direction normal to the surface due to the confinement of chains inside the layer could be the reason for this. However, effects such as disruption of 3D topology appear unrealistic in the system, given that the relaxation dispersion shape of the films remains bulk like and

that the polymer is poorly wetting (see below).

Apart from the pore diameter (confinement size), the curvature of the pore surface is an important factor determining the chain dynamics in these films. As the pore curvature approaches the coil dimensions, the radius of gyration R_g, coupled with the high entropic penalty and the enthalpic disadvantage (especially, if polymer is poorly wetting) imposed on the chains to spread onto the surface, may result in favoring the chains to actually form thicker layers in contrast to the anticipated layer thickness. This in turn results in a more bulk like state for the chains. One important factor to consider here is the interactions of the polymer with the surface. If the wettability of the polymer with the surface is low, the layer formation process is retarded due to high enthalpic disadvantage of spreading resulting in both the size effects as well as the adsorption effects becoming weak.

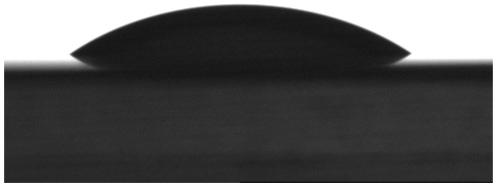

Figure 6.3 : *A Polybutadiene droplet on the surface of γ-alumina. The droplet shows poor wetting characteristics thereby not spreading evenly on the surface as expected for a polymer with good wetting characteristics like PDMS.*

In order to examine the wettability, a polybutadiene droplet, spreading on a flat alumina surface was observed under an optical microscope. The droplet is shown in fig 6.3. Clearly seen is the non-spreading behavior of the melt with a high contact angle showing poor wetting characteristics of PB melt on alumina. The droplet did not evolve into a flat profile for over 12 h. Such a behavior is in contrast to PDMS which forms a macroscopically uniform thin layer (data not shown) almost instantaneously. The high hydrophobicity and the non-existence of interacting species (like -Si-O- groups in PDMS) renders the polymer poorly wetting on the hydrophilic alumina surface.

Such non-wetting properties preventing spreading of the molecular layer results in non-uniform distribution of the layer. This in turn renders the actual dimension of the layer much larger than that expected from a uniformly distributed layer. This explains the non-observation of deviation from bulk and rather only a reduction of relaxation times from the bulk even at very low expected coverages.

In the 20 nm pores (cf.fig.6.2b), decreasing surface area available in a smaller pore results in smaller area for adsorption. Additionally when the surface curvature approaches the bulk polymer size (R_g), the tendency of the melt film to form blobs or in other words the energy penalty involved in spreading is enhanced resulting in a thicker bulk-like layer than expected. In such bulk-like layers, the motions are obviously much less restricted. This explains the observation of bulk-like behavior in films whose layers are far more thinner than the ones in 200 nm pores. In such smaller pores, the larger curvature aids the non-spreading of the melt resulting in a thicker layer than expected, even for sub-nm layers.

6.2.2 PB in Nanoporous Silica

Commercially available porous silica (96%) substrates known as *Vycor* with a mean pore diameter of 4 nm was used to confine PB2k melts. The average pore diameter as specified by the manufacturer is only slightly larger than the radius of gyration of the polymer used (R_g=2.2 nm) [66]. Thus the effects of confinements is expected to be stronger compared to films in alumina substrates (A200 and A20) discussed in the previous section. As discussed above, the relaxation dispersion of the bulk melt with molecular weight being below the critical molecular weight M_c (4000 g/mol) [49], follows Rouse dynamics [15]. The relaxation dispersion of the samples formed by partial loading of PB melt in the pores is shown in fig.6.4. Alongside, dispersion of PB2k bulk as well as another sample where the substrate is completely filled with the melt is also shown. The dispersions clearly show deviation from bulk for all the samples with an increased power law of about $\nu^{0.5}$. While the power law remains deviant from the bulk and the same for all the samples, the absolute relaxation times are slightly reduced for samples with decreasing polymer loading.

Similar to several of the above mentioned studies [60, 63, 68], with a slope of 0.5, the dispersion shape corresponds to limit III of the Doi-Edwards theory (see §3.6). However, the predominant relaxation mechanism as shown by Kimmich et al. is not ordinary reptation as proposed by the tube model [18] but the reptating polymer moving in a correlated manner. Such a mechanism has been shown not to violate the governing thermodynamic principles, while maintaining the signatures predicted by the limit III of the Doi-Edwards Model in the time regime $t \gg \tau_R$ [68]. The contributions in this region are therefore mainly intersegmental in nature. The surface interactions play a major role in this system as shown by the strict observance of the predicted slope of 0.5, unlike in other systems [60, 63], where either weak or no interaction with the substrates results in the reduction of the characteristic time constants diluting the observed slope.

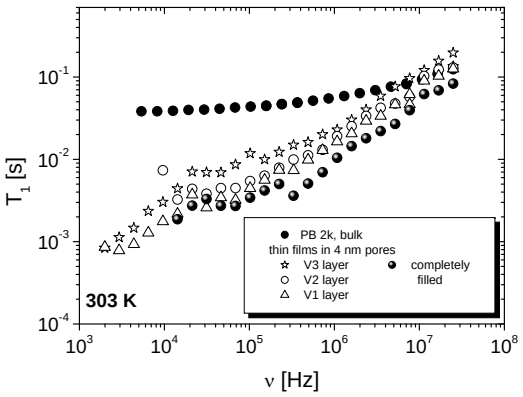

Figure 6.4 : *Polybutadiene melt films in partially filled vycor substrates along with the relaxation dispersion of the bulk for comparison.*

Another interesting phenomenon is the reduction of relaxation times at low frequencies depending on the amount of polymer loading. With decreasing polymer loading, the degrees of freedom for the chain motion increases resulting in an increasing relaxation times, although the relaxation mechanism remains the same. This is similar to the relaxation dispersion study of varying amounts of perfluoropolyether in Vycor [59], where the loaded amount was controlled by varying the immersion time of the substrate in the melt, while in this study, the same was controlled by varying the solution concentration. Additionally, with increasing polymer loading, the number of adsorbed chain segments may increase, thereby reducing mobility.

6.3 Conclusions

Polybutadiene, a highly hydrophobic polymer was studied inside pores of alumina and silica of various sizes. In alumina, the relaxation dispersion showed a layer thickness dependent reduction in relaxation times, specially at lower frequencies corresponding to motional restrictions of slower motions, while motion at high frequencies remain less affected. The qualitative behavior did not change for any of the samples. The polymer showed extremely poor wetting properties, which could have resulted in formation of blobs, specially when the radius of curvature increases like in smaller pores. This explains the non-deviation from bulk of even nominal sub-nm films.

In Vycor, the porous silica substrate, the chain motion followed a special kind of reptation, that is correlated motion of segments, as has been observed in systems which show

good interaction between polymer and the substrate. With decreasing polymer loading, the number of degrees of freedom for motion increases resulting in increasing mobility in the range studied.

Chapter 7

Dynamics of Poly Dimethyl siloxane thin films in nanoporous media

7.1 Introduction

Polymers at interface are a subject of intense research over the years for both its industrial application as well as scientific research potential. Interfacial chains have been known to affect properties especially when the length scale of the system approaches molecular dimensions, like in the case of thin films [11, 69, 70, 71]. It has previously been discussed that interfacial forces affect the dynamics of polymer chains in a wide range of time scales, for instance, from long-time scale processes such as diffusion [72, 73] to medium time-scale processes such as Rouse modes. With dynamics of polymers in thin films as well as in other confined systems spanning many orders of magnitude in frequency, it becomes important to investigate the motions of polymer chains on time scales as wide as possible.

The polymer film system that was chosen for investigation was polydimethylsiloxane (PDMS) adsorbed on porous alumina. PDMS is considered a model polymer in many cases for its linearity and uncomplicated structure, molten state at room temperature. Investigations on PDMS is also advantageous considering its industrial applications ranging from tyre industry to cosmetics to microelectronics. The substrate, porous alumina membrane discs, is formed by Anodization of aluminium. It is hydrophilic in nature with the pores as cylindrical channels of defined size and structure running parallel throughout the membrane thickness. The hydrophilic nature of alumina and the hydrophobicity of PDMS results in a weakly adsorbing polymer system. Such systems are characterized by weak adsorption strengths, anomalous equilibrium kinetics, low surface residence time, and fast exchange between adsorbed and non-adsorbed chain segments [74]. Thus the motional heterogeneity normally expected in thin films, might be more pronounced in this case.

Some earlier studies on PDMS thin films have confirmed that PDMS can form flattened configurations in a monolayer, whose thickness on different substrates [75] [76] is 0.7 nm. In ultrathin films [11], surface induced ordering takes place up to at least 2 monolayers, where 3 distinct dynamic environments were observed, while surprisingly in thicker films ($>$ 8 nm) [10], such heterogeneities disappear. Multiple quantum (MQ) NMR [77] was

used earlier in the same system and it is claimed that the observed multiple peaks of the MQ build-up arrives from heterogeneous dynamic environments of individual monolayers. Another useful study on PDMS includes one by Litvinov et al. [78] who have modelled PDMS chains grafted onto silica particles into 3 distinct regions accounting for the observed dynamics using transverse relaxometry.

Taking into account these findings, some of the objectives of the study are as follows: to extend the above mentioned findings for the case of a weakly adsorbed polymer thin film system; to see the effect on dynamics owing to the confinement of chains in thin layers; to study the influence of the curved interfaces in comparison to the flat substrates; to study the influence of surface chains on the properties such as entanglements; to study the transition from bulk to confined dynamics and to finally come up with a model explaining the dynamical behavior in these thin films. To this effect, PDMS thin films of various molecular weights below and above the entanglement threshold, formed in porous alumina as a function of film thickness in two different pores sizes were examined. The results are complemented by other methods viz. transverse relaxometry and DQ NMR. Finally, in an effort to explain all of the observed properties, a tentative model on this system is arrived.

7.2 Experimental

PDMS with three different molecular weights (10k, 30k and 200k) were used in the study to prepare thin films in porous alumina of pore sizes 20 nm and 200 nm. The samples were prepared and characterized as explained in §5.2.1. The average nominal film thicknesses obtained from tabulated densities and sample weights are given in table 7.1 for the PDMS samples of this study.

Table 7.1 : *PDMS thin films of various nominal layer thicknesses confined inside Anopore membranes. The constants used in the calculations are as follows: ρ(PDMS)=0.97 g/cm^3, ρ(Alumina)=3.423 g/cm^3, monolayer thickness=0.7 nm.*

Sample	Pore Diameter (nm)	Average weight of membranes (mg)	Average weight of poly/mem (mg)	Nominal film thickness (nm)
PDMS10k	200	82.20	0.56	0.45
	200	87.20	0.70	0.57
	200	83.40	1.80	1.20
	200	78.60	2.20	1.70
	200	85.10	3.05	2.56
	200	75.50	3.97	3.00
	20	130.40	1.56	0.16
	20	122.50	2.40	0.20
PDMS30k	200	84.70	1.56	1.26
	200	81.80	2.70	2.10
	200	79.10	5.56	4.50
	200	76.50	6.41	7.10
	20	127.60	1.26	0.13
	20	124.20	1.53	0.15
	20	126.10	4.90	0.50
PDMS200k	200	63.25	4.43	3.30
	200	85.78	1.40	1.13
	200	82.23	2.03	1.50

7.3 Results

In the following sections, results of the relaxation dynamics of PDMS thin films in 20 nm and 200 nm pores investigated using FFC at different temperatures are presented. Results from additional investigations viz. transverse relaxometry and proton double quantum NMR for the quantification of residual dipolar couplings are also presented.

7.3.1 Relaxation dispersion of PDMS thin films

The relaxation dispersion of the thin films of PDMS10k with different nominal layer thicknesses are given in fig. 7.1 along with the dispersion of the bulk for comparison. The bulk, with molecular weight below the critical molecular weight ($M_w < M_c$; M_c^{PDMS}=25000 g/mol [49, 50]) follows Rouse behavior like other melts [15, 35]. The nominal thickness of the

samples used in this study, in terms of number of monomeric layers, corresponds to a range between several monolayers to sub-monolayers, given that the monolayer thickness of PDMS films formed on solids [76] and liquids [75] with flattened chain configuration is about 0.7 nm. In the limit approaching sub-monolayer thickness, strong deviations might be expected from bulk behavior owing to a crossover from 3D to 2D topology.

As seen from the figs. 7.1 and 7.2, the relaxation times of the thin films are smaller than the bulk for all the studied samples. As the layer thickness becomes smaller, this effect becomes more pronounced and at sub-monolayer coverages, the dispersion shape is no more bulk-like.

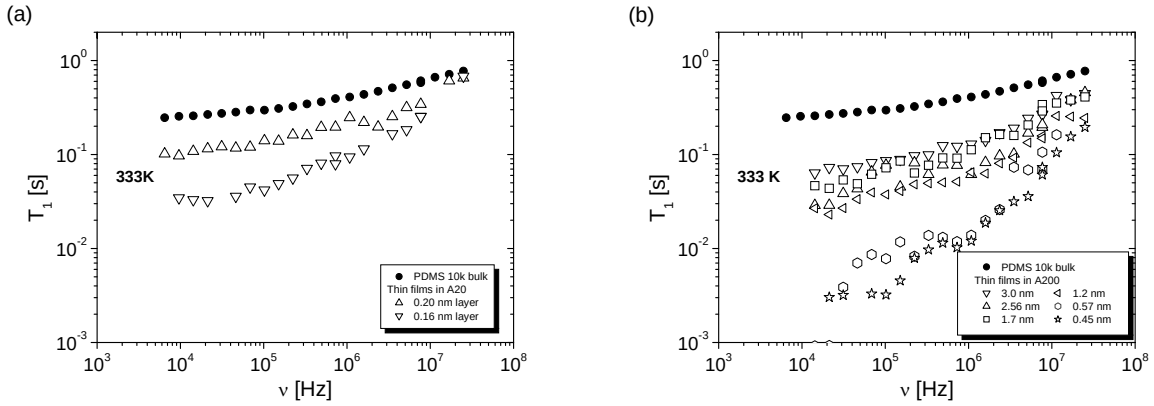

Figure 7.1 : ^1H T_1 *relaxation dispersion profiles of PDMS10k samples of different nominal layer thicknesses, confined in (a) 20 nm pores and (b) 200 nm pores along with the bulk for comparison.*

In detail, for the PDMS10k thin films in 20 nm pores (fig. 7.1(a)), the relaxation times shows a reduction by a factor of 3 and 8 respectively for the 0.2 nm and 0.16 nm layers at a frequency range of about 20 kHz. At high frequencies (>10 MHz), the relaxation times tend to converge to that of the bulk. This shows that the slow molecular reorientations probed in the kHz frequency range are more restricted, yet no qualitative deviation from the bulk dispersion shape is observed even for samples with nominal thickness ranging between 0.2 and 0.3 monolayers in these small pores (A20).

The relaxation dispersions of a wider range of PDMS10k thin films in A200 (fig.7.1(b)) studied here show different effects due to confinement. The relaxation times for the films

at a frequency of about 20 kHz is reduced by 1-2 orders in magnitude depending on the film thickness. A factor of 1-2 in reduction at the highest frequencies is also seen, which is more pronounced compared to the films in A20. Most importantly, while the thicker films retain bulk-like dispersion shape, the relaxation dispersion of the 0.57 and 0.45 nm films, the thinnest films in the series, show a deviation from the bulk behavior. Rather than tending towards a plateau at frequency below 10 MHz, the relaxation dispersion for these films shows an increase in the slope. Deviations of confined melts from bulk behavior have been observed previously [59, 60, 39] when they are fully confined in solid impenetrable walls in the range of the molecular size (radius of gyration, R_g) and are explained by the *tube/reptation* [17, 18] model. The difference here is that neither the confinement is of the molecular size, nor is the polymer completely filling the void pore but forming a thin film.

The relaxation dispersion of PDMS30k thin films are shown in fig. 7.2 along with the bulk melt. With the molecular weight of the bulk melt exceeding the critical molecular weight ($M_w > M_c$), the relaxation dispersion for PDMS bulk melt in the probed frequency range corresponds to limit II of renormalized Rouse formalism [36], according to which, a power law of 0.25 is predicted and is reflected in the measured profile of the bulk. With stronger intermolecular interactions (entanglements) in this sample, the effect of confinement might be of a different nature, especially in ultrathin films, where isolated chain segments may show weaker entanglement effects.

The relaxation dispersion of the PDMS30k thin films at first look appears qualitatively similar to the bulk with a mere reduction in relaxation times, apart from the transition region above several MHz in frequency, being shifted towards smaller T_1. This is the case for films in both larger (A200) as well as smaller (A20) pores, where sub-monolayer coverages have been investigated only in A20. However, a more detailed analysis shows that the relaxation dispersion of the thinnest films in A200 deviate from the bulk with an increased slope. The 1.25 nm film and the 2.1 nm films in A200 show a somewhat increased power law $T_1 \propto \omega^{0.35}$, indicating a deviation from bulk behavior, while such a change is not observed for the thicker

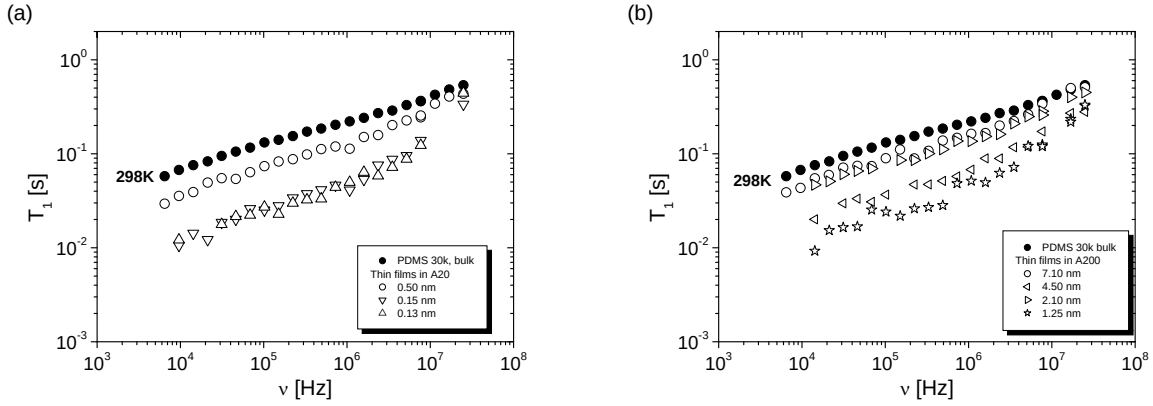

Figure 7.2 : ^1H T_1 *relaxation dispersion profiles of PDMS30k samples of different nominal layer thicknesses, confined in (a) 20 nm pores and (b) 200 nm pores respectively. The relaxation dispersion of the bulk is given for comparison.*

films. More information on the behavior of these chains using field cycling relaxometry can be obtained by studying the temperature dependence of relaxation profiles.

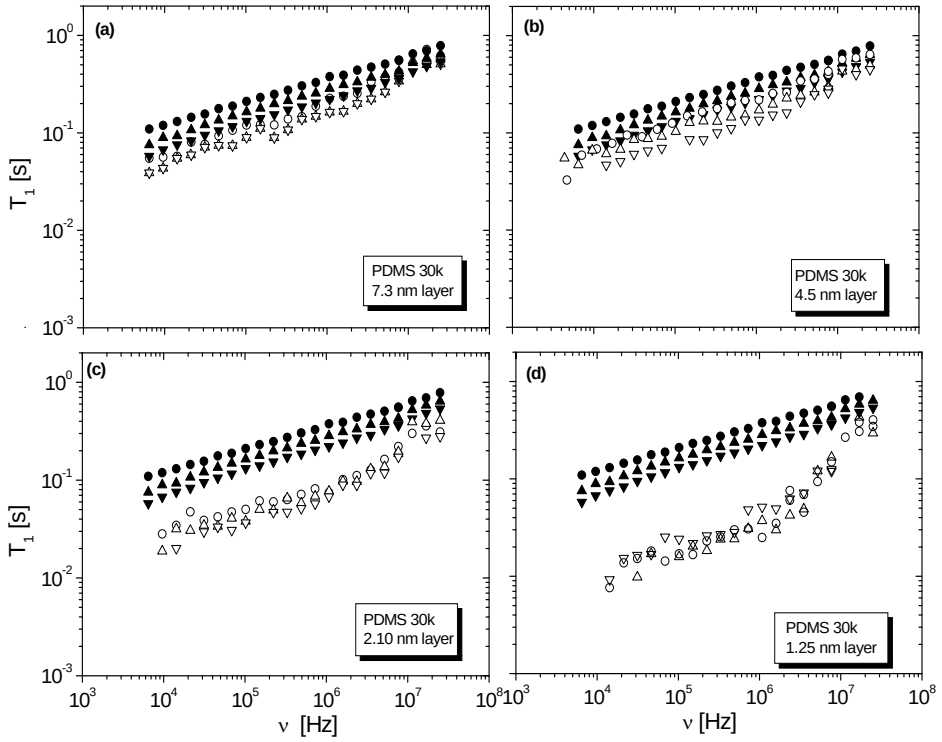

Figure 7.3 : ^1H T_1 *relaxation dispersion profiles of PDMS30k thin films in A200 at different temperatures. The symbols correspond to the temperature as follows:* $(\bullet, \circ)$*:333 K,*$(\blacktriangle, \triangle)$*:313 K and* $(\blacktriangledown, \triangledown)$*:298 K.*

In fig. 7.3, the temperature dependent profiles for PDMS30k thin films in A200 are

presented. The samples correspond to a range from about 10 (7.1 nm layer) to about 2 monolayers (1.25 nm layer), considering the monolayer thickness of PDMS being 0.7 nm [76, 75].

The temperature dependence of relaxation profiles of the 7.1 nm and 4.5 nm layer corresponding to 10.1 monolayers and 6.5 monolayers nominally, shown in fig.7.3(a),(b) is similar to that of the bulk. At the same time, the dispersion shape remains essentially unchanged, following a power-law behavior similar to that of the bulk ($T_1 \propto \omega^{0.25}$) below 10 MHz.

Temperature dependent relaxation profiles for the thinner films however, resulted in a different scenario. Shown in fig.7.3(c),(d) are the temperature-dependent profiles of the sample with a nominal layer thickness of 2.10 and 1.25 nm, respectively corresponding to 3 and 1.8 monolayers respectively. The 2.1 nm layer shows a deviation from the bulk behavior with an increased slope ($\propto \omega^{0.35\pm0.06}$) at 298 K but with increase in temperature approaches bulk behavior, and at 313 K shows a slope of about ($\propto \omega^{0.29\pm0.04}$) below 3 MHz. The 1.25 nm layer shows a weaker temperature dependence compared to the other layers and an increased slope ($\propto \omega^{0.37\pm0.08}$) in the whole temperature range unlike the 2.1 nm layer. The reason for the different behavior between the samples in the range from about 10 to 2 monolayer nominal thickness is probably related to the more pronounced geometrical restriction of the thinner samples and to the reduced mobility of adsorbed segments.

Field cycling profiles were also measured for a high molecular weight PDMS200k to investigate the effect of confinements on the entanglements. The figure 7.4 shows the temperature dependent relaxation dispersions for two of the PDMS200k thin films formed in A200 along with the dispersion of PDMS30k bulk as reference. It is theoretically known [36] as well as experimentally observed [35] that for polymers with $M_w > M_c$, the slope of the region observed in this frequency regime for the bulk polymer is independent of the molecular weight.

The profiles for the 1.13 nm layer shows a significant deviation from bulk with an increased power law ($\propto \omega^{0.45\pm0.1}$), but a tendency towards a weaker frequency dependence at increasing

temperatures is seen. For this higher molecular weight, even the 3.3 nm layer shows a slight change in the slope, which is less pronounced at lower temperatures. Thus deviation is seen for all the samples, even for this high molecular weight.

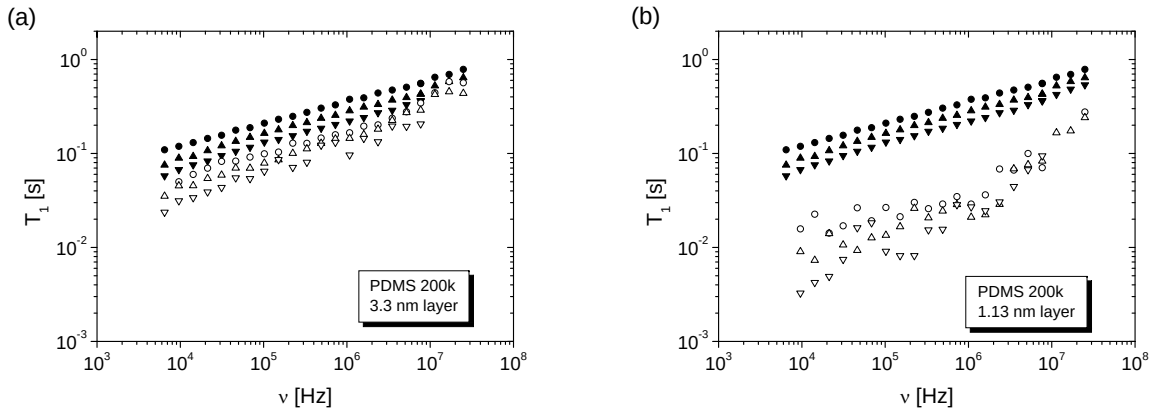

Figure 7.4 : *Temperature dependent relaxometry profiles of PDMS 200k thin layers (open symbols) in A200 (a)3.3 nm layer and (b)1.13 nm layer, along with the PDMS 30k bulk (closed symbols) at 298 K(▼, ▽), 313 K(▲, △) and 333 K(●, ○).*

The above results are discussed in detail later. In the next section, complemetary results from transverse relaxatometry and double quantum (DQ) NMR are presented.

7.3.2 Transverse relaxation and ^{1}H Double Quantum build-up of PDMS thin films

While T_1 dispersion investigates chain reorientation motion in the frequency scale of the applied magnetic field (Larmor frequency), transverse relaxation (T_2) gives information about integrated slow motion components. T_2 relaxation of all thin films investigated using Carr-Purcell-Meiboom-Gill (CPMG) pulse sequence, that mainly probes uncoupled spin pairs, showed multi-exponential relaxation behavior, irrespective of the molecular weight and layer thickness. These curves were best fitted with a bi-exponential fit, while higher order exponential fits did not reduce the residuals significantly. The description of relaxation curves using two exponentials may symbolize the existence of at least two components of distinct mobility, however a continuous distribution of relaxation components as well as other shorter

relaxation components cannot be ruled out.

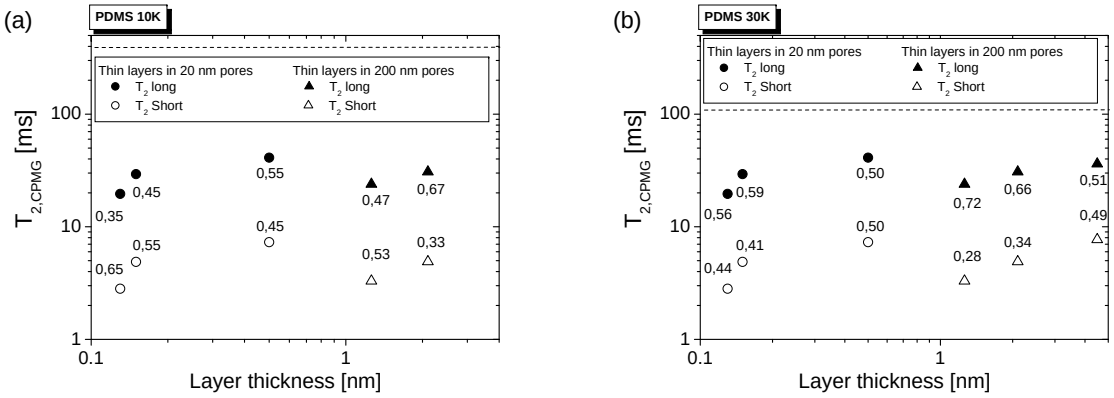

Figure 7.5 : *Analysis of transverse relaxation data for different samples of (a) PDMS10k and (b) PDMS30k. The long component and the short components along with its weight fractions (numbers above and below) from a bi-exponential fit to the relaxation decays are given. The dashed horizontal line corresponds to the bulk value in the respective figures. All measurements were carried out at a* ^1H *Larmor frequency of 200MHz and at 298 K.*

The analyzed results including the relative weight of each fraction (numbers below data points) of the transverse relaxation experiments on PDMS thin films performed at 298 K are presented in fig.7.5. The transversal decay of the PDMS10k bulk showed mono-exponential behavior while PDMS30k bulk, whose molecular weight is only slightly higher than the critical molecular weight, showed only a slight deviation from mono-exponential behavior; the horizontal lines in the figure denotes these bulk values, given here for comparison.

The T_2 values for all the thin films show a marked decrease in comparison to the bulk values (325 ms for PDMS10k bulk; 109 ms for PDMS30K bulk). The shortest values are obtained for the thinnest films and are reduced by up to two orders of magnitude. However, the long component values are comparable to highly mobile chain segments of dangling ends or long loops observed in grafted PDMS chains upon swelling by a solvent [78].

On a closer look, results from PDMS10k thin films show a trend of decreasing T_2 (both long and short) with decreasing coverage. However, T_2 from equivalent thin layers in pores of different sizes cannot be compared, since a distinct dependence on the pore size becomes evident. The above mentioned observations of dependence of relaxation times with layer thickness and with pore size follow the same trend as the relaxation dispersion data. With

respect to the weight fractions, the short component (A^{short}) that corresponds to less mobile chain fractions, increases with decreasing layer thickness. A simple attribution of each value to two fractions, one bound to the surface and another mobile and free, is not possible though, considering the relationship between the weight fraction and layer thickness (no inverse proportionality).

For the PDMS30k thin films, the results are similar to those of the PDMS10k thin films. Although the bulk relaxation values of the two molecular weights differ by a factor of 3, the values of relaxation times of thin films of the two molecular weights, appear to be similar. Similar to PDMS10k films, with decreasing layer thickness, the relaxation times of the shorter component increases and the weight fraction of the shorter component decreases, indicating higher fraction of restricted segments in thinner layers. In both the relaxation dispersion results as well as the transverse relaxation results, clearly, a dependence of pore size appears, preventing the comparison of these results from similar layers in the two different pores. Additional results from solid echo decay curves for PDMS30k samples confined in A200 were also recorded and are presented in the last part of this section.

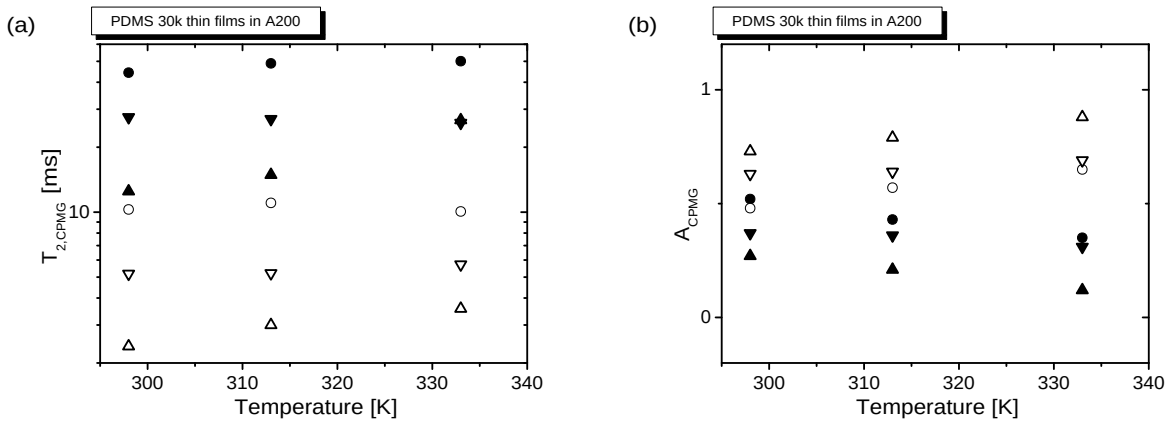

Figure 7.6 : *Temperature-dependent plots of (a) Transverse relaxation times ($T_{2,CPMG}$) and (b) weight fractions(A_{CPMG}) obtained from fits of CPMG decay curves for PDMS30k thin layers;(●)-4.5 nm layer, (▼)-2.1 nm layer and (▲)-1.25 nm layer. The closed and open symbols correspond to long and short components, respectively. The errors for the relaxation times/amplitudes were smaller than the symbols themselves.*

The temperature dependence of transverse relaxation was measured using CPMG as well as solid echo (SE) pulse sequences. The transverse relaxation times of PDMS30k samples measured at various temperatures with CPMG pulse sequence is given in fig.7.6. In general, in the range of the temperature studied, the relaxation times are not affected drastically, increasing by only a factor up to 2. The most significant dependence on temperature on a relative scale is observed for the sample with the smallest polymer amount, while the remaining samples show only a very weak temperature dependence at most. At the same time, the relative weight fraction of the short component (A_{CPMG}^{short}) steadily increases for all the samples. The absolute values even at higher temperatures are still lower than the bulk value at 298 K.

Segments adsorbed on pore walls have reduced mobility due to surface interactions, thereby rendering intermolecular dipolar interactions to be only partially averaged. In order to obtain information about such partially averaged dipolar couplings, the study of solid echo (SE) decay is known to be a very useful method [78] since strong incomplete bilinear dipolar interactions are effectively refocused by the SE. The transverse relaxation components of such systems are characterized by times in the range from a few microseconds up to a few milliseconds.

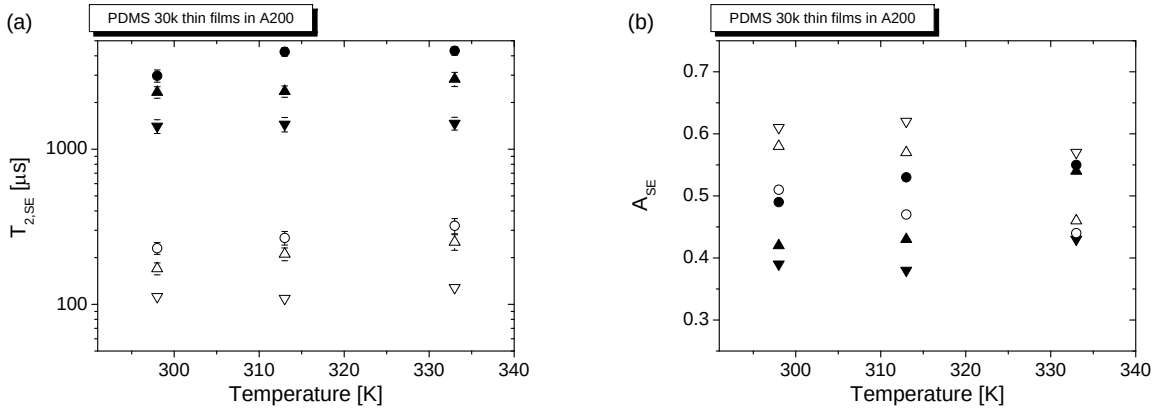

Figure 7.7 : *Transverse relaxation times (a) and weight fractions(b) obtained from fits of Solid-echo decay curves for PDMS30k thin films. As in fig7.6, the symbols (●, ▲, ▼) correspond to 4.5 nm, 2.1 nm and 1.25 nm layers. The open and close equivalents correspond to short and long components respectively.*

The analysis of solid echo decay results are given in fig. 7.7. The shortest relaxation component is observed for the thinnest layer (T_2=102 μs). Compared to a T_2 of 70-90 μs relaxation times observed for PDMS chains grafted on silica, the chains in the system, at least in the thinnest layers are not so much more mobile. However, a Gaussian component as expected for a solid with unaveraged dipolar interactions, could not be identified.

The short and the long components are almost an order of magnitude different. The relaxation times in general, show a strong dependence on the layer thickness, specially the long component while the short component amplitude also increases with decreasing polymer loading, corresponding to an increased fraction of restricted segments.

With increasing temperature however, there is only a weak change in the long component, while the short component increases notably, specially for the thicker film. The most significant change is for the change in amplitude of short component.

On the whole, as a general feature, one finds that a temperature dependence in the range 298 to 333 K is almost absent for the thinnest layer but gradually becomes stronger with increasing polymer amount. This is similar to the trend found in the results from field-cycling relaxometry.

To get information on the motionally restricted strongly coupled spins, double quantum NMR that effectively accesses the residual dipolar couplings, prevalent in partially dipolar averaged systems such as thin films, is used. The double quantum intensity build-up for two representative PDMS30k thin films in A200 and A20 pores each are shown in fig.7.8.

From the build-up curves, the first order maxima for the samples from the DQ build up curves occured at approximately the same excitation interval. The intensity for the thinner layers though was much higher than that of the thicker layers. The peak intensity is related to the strength of the dipolar coupling while the position of the maxima is an interplay between the DQ buildup intensity and the single quantum transverse relaxation decay of the spins [79]. The build-up curves showed well-resolved multiple peaks as obtained by Jagadeesh et al. [77] on the same system. As interpreted by them, these peaks are manifestations of

DQ coherence build-up from different layers in a multi-layered film.

The residual dipolar coupling (RDC) constants obtained from the slope between signal intensity and excitation/reconversion times are presented in table 7.2. The residual dipolar coupling constants are a measure of coupling strength between spatially correlated spins, the correlation induced by motional restrictions, and have been successfully used to characterize systems like elastomers [79].

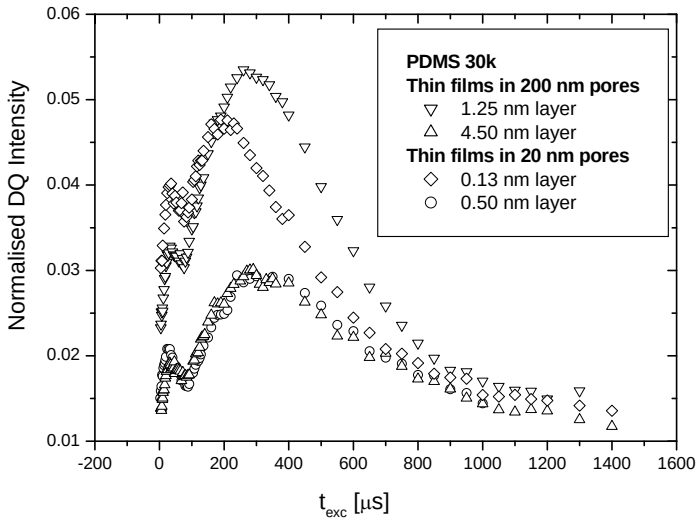

Figure 7.8 : *Double quantum build-up curves as a function of the excitation time, obtained using the 5 pulse experiment.*

The RDC constants for the bulk melt are almost negligible, since the dipolar couplings are almost completely averaged owing to high flexibility and low viscosity of the melt as in the case of simple isotropic liquids. Thus the RDC observed for the thin films directly probe the molecular order induced by the interactions of the pore wall and the pore confinement effect. For both PDMS10k as well as PDMS30k thin films, the highest RDC constant is observed for the thinnest films. In general, the RDC constant decreases with increasing layer thickness indicating decreasing molecular ordering and dynamic restrictions. Along with the pore size dependence, these results show the same trend as the findings from relaxometry.

In all of the above investigations, although sub-monolayer thin films can be easily inves-

Table 7.2 : *Residual Dipolar Coupling (RDC) constants of various confined samples of both PDMS10k and PDMS30k polymers, calculated from the slope of the initial linear part of the build up curve.*

	Pore diameter (nm)	Layer thickness (nm)	RDC constant (Hz)
PDMS	bulk		0.25
10k	200	0.45	793
	200	0.60	575
	200	2.50	312
PDMS	bulk		30
30k	200	1.26	667
	200	2.10	436
	200	4.50	278
	20	0.13	590
	20	0.15	436
	20	0.50	305

tigated only inside smaller pores, since the larger curvature of the 20 nm pores was in the same order as that of the polymer radius of gyration(R_g) which happens to be 3 nm, 5 nm and 12.5 nm for PDMS 10k, 30k and 200k respectively, it was suspected that the melt may really not form a film of thickness as expected. This can be clearly seen from the bulk-like behavior of even sub-monolayer films (a '0.5 nm' thick PDMS30k films in A20, nominally a sub-monolayer film behaves bulk-like). Hence the films formed inside 200 nm pores were more likely to be flat.

7.4 Discussion

The broad aim of this study is to investigate the highly intriguing dynamic processes in thin films using the rich and developed set of NMR methods. Classically, polymer thin films are considered to be a microscopically smooth layer forming on a flat planar substrate, however the limited sensitivity of NMR (especially at low field) requires the use of porous substrates with high surface/volume ratio, which when partially loaded, allow one to investigate thin films using methods like low field NMR. Though polymers have been investigated previously

in pores using field cycling NMR, most of the studies have concerned pore-filling scenario i.e. polymers completely saturating the void space of porous matrices [68, 80, 62] or being contained between sheets of impenetrable foils [41]. In all cases, confinement was found to affect the reorientational dynamics, even when confining dimensions are in the order of μm which far exceeds the characteristic chain dimensions. Interactions were interpreted in terms of coherent effects mediated by the compressibility of the polymer melt [81].

The studied system of the polymer forming a layer inside pores might include effects such as enhanced mobility due to the free air-polymer interface, restriction due to confinement in pores as well as other effects due to pore curvature. A number of questions have to be asked at this stage: at what length scales do the chains deviate from bulk behavior and what are the underlying reasons? How important is the pore curvature and at what length scale can one expect chains not to 'feel' the curvature? How mobile are the surface molecules: are they rigidly bound or are they mobile and diffuse freely or does this feature have a dependence on other parameters such as layer thickness? How are conformations and dynamics affected for polymer concentrations which are insufficient to provide a complete coverage of the surface?

From the results, a common observation is that T_1 at frequencies above 10 MHz is only slightly reduced, specially for thicker films. This frequency range corresponds to the (semi-local) fast anisotropic segmental reorientation motion. The results show that these fast motions are essentially unaffected by pore geometry as well as by the surface interactions. Relaxation times in the range 10^5 to 10^7 Hz are most affected for all samples, in general; in bulk, this range corresponds to chain mode regime comprising a major but not the whole part of the chain as well as majorly intra-segmental interactions. Entanglements and other intermolecular interaction effects are expected only for polymers with molecular weight higher than the critical molecular weight, and even in that case, are expected only to appear in the spectrum at much lower frequency. Thus a straight forward interpretation for the relaxation data should be the slowing down of motions accompanied with a change in the relative weights of the motional modes.

At a closer look, the profiles of PDMS30k thicker layers in A200, the 7.1 nm and 4.5 nm layers corresponding to 10.1 and 6.5 monolayers respectively ($d^{PDMS}_{monolayer}$=0.7 nm), show bulk-like behavior from the dispersion slope with reduced relaxation times, while the thinner layers show a change in the slope with a tentative deviation from bulk. A similar behavior is also seen for PDMS10k films in A200, where the thicker films behave bulk like while the thinner films show a deviation from the bulk with an increased slope. This effect will be discussed with profiles measured at different temperatures along with transverse relaxometry measurements shortly.

CPMG pulse sequence provides information on uncoupled mobile spin pairs. The relaxation decays are best fitted with a second-order exponential function. From transverse relaxation times measured with CPMG, chain mobility shows a tendency to decrease with decreasing layer thickness due to the increase in motional restrictions. It is however interesting to note that the longest relaxation times are in the same range for thin films of both the molecular weights, while their bulk values differ by a factor of about 3, implying that the mobility restrictions in these films could be molecular weight independent, although the underlying processes could be different, for instance, a change in the effect of entanglements can take place only in PDMS30k films. Regarding the weight fractions, the short component weight fraction is also seen to be decreasing with increasing layer thickness signifying higher fraction of mobile chain segments with increasing layer thickness due to the obvious decrease in surface space available for the chain segments to adsorb.

SE relaxation curves were also best described by second order exponential function. Relaxation times from SE provide information about mobility of strongly restricted segments. The shortest relaxation time observed for any sample is about 100 μs for PDMS30k 1.25 nm layer, which is only slightly higher compared to grafted PDMS segments on silica (60-80 μs) [78]. Thus the adsorbed chain segments in the thinnest films do not appear to be extremely mobile, however, a Gaussian component is not observed here, which is expected for unaveraged dipolar interactions [78].

The relaxation decays are best fitted with a second-order exponential function. The two components however cannot be simply decomposed and assigned to adsorbed and non-adsorbed segments for the following reason: the system of PDMS adsorbed on alumina represents a weakly adsorbed polymer system [82]. Such systems are characterized by weak bonding forces such as van der Waals forces, different equilibrium kinetics, low surface residence time, and fast exchange between adsorbed and non-adsorbed chain segments [74]. These factors render the fraction of adsorbed chain segment per chain, a variable with a large distribution [83, 84], making the assignment doubtful. However, the two transverse relaxation components may refer to two populations with a broad distributions of mobility each, one more restricted -close to the surface and the other less restricted -far from the surface.

The residual dipolar coupling constants give an idea of the anisotropy in mobility and order in the system. However, with the samples being unoriented, the RDC constants give information about the immobility itself. The RDC constants found from the DQ build up curves decrease with increasing layer thickness. These results complement the results from other measurements that due to a higher fraction of adsorbed chains and stronger confinement effects the mobility decreases with decreasing film thickness.

In all of the above measurements viz. longitudinal, transverse relaxometry and DQ NMR, a distinct dependence of dynamics on pore size is evident. While films that are 1-2 monolayers thick in 200 nm pores show stronger dynamical effects in comparison to films that are even sub-monolayer thick in 20 nm pores. The difference is the pore curvature and the related energy of the molecules to spread on to a film. For the bulk size of the molecules used in the study (PDMS R_g^{10K}:3 nm, R_g^{30K}:5 nm, R_g^{200K}:12.5 nm), the 200 nm surface appears more flat compared to the 20 nm pore surface. The stronger curvature of the smaller pores results in higher energy required for the molecules to spread on the surface, preventing chains from forming a flat film in 20 nm pores. This results in the bulk-like behavior of even the nominally sub-monolayer films in 20 nm pores.

The temperature dependence of relaxometry profiles provide interesting information on the dynamics of these systems. From the relaxation dispersion results of PDMS30k films (see figs.7.2,7.3), the bulk melt shows a dispersion slope of 0.25 in accordance with limit II of the renormalized Rouse theory [36](see §3.5). The chains in the 7.1 and 4.5 nm thick layers do not undergo a qualitative change in behavior relative to the bulk over the studied temperature range, obeying the same power law as the bulk. However, in the case of the thinner films, the 2.1 nm layer shows a deviation from bulk in the form of a slight change in the slope of the relaxation dispersion at lower temperatures, while showing a tendency toward bulk behavior at higher temperature. In the case of the 1.25 nm layer, the dispersion shows deviation from bulk at all temperatures studied. The temperature dependence of the profiles of the different samples decreases with decreasing layer thickness, as can be seen from fig. 7.3. The profiles for the 7.1 and 4.5 nm layers show similar temperature dependence as compared to the bulk, while the 2.1 and 1.25 nm samples, the thinner samples in the series, show a slightly weaker temperature dependence. Reptation dynamics observed for strongly confined chains however, is not observed even for the thinnest films; the free-air interface being a region of enhanced mobility is a clear violation of the conditions required for reptation.

In adsorbed chain systems such as in thin films, a part or the whole of the chain exists in the adsorbed state, while the rest of the chain exists as free non-adsorbed chains. However, the non-adsorbed chains are still motionally restricted due to the connectivity with the part that is adsorbed. The difference between the two parts is the degree of motional restrictions and the ensuing effects. While the segments of the chain that are adsorbed might not only be severely restricted but due to the accompanying structural changes might show non-bulk-like properties. Concepts such as *dead layer* [72, 85], *reduced mobility layer* [86] etc are now well known dynamic features observed in thin films. This is related to chains close to the surface that are severely restricted in motion, affecting chain properties like diffusion [73], local segmental mobility [87], glass transition [88] etc. The width and the nature of this mobility

restricted region along with the ensuing effects is a field of ongoing research. The extent to which each property is affected depends on the perturbation length of the restricted layer and the property itself, and the intrinsic properties of the system like the polymer flexibility, surface interactions, temperature etc. Any measured parameter of these chains is then a convolution of the properties of these two kinds of chains.

The longitudinal relaxation times (T_1) of a chain are an unresolved weighted average of the two components due to chain connectivity, i.e., the same chain where one part is adsorbed and the other is non-adsorbed, as seen from a single exponential longitudinal relaxation curve. The effective observed T_1 of the system thus depends on the contributions from the two regions: a region close to the surface, whose dynamics are influenced by the adsorption of the chains, henceforth mentioned as *adsorption restricted layer* or ARL and a region far from the surface, whose dynamics are restricted due to chain connectivity and henceforth mentioned as *connectivity restricted layer* or CRL. The chains in ARL follow non-bulk like dynamics due to a tentative change in chain conformations. The thickness of this ARL should be of the same order as the length scale at which deviation in relaxation dispersion occur.

The change of slope from the theoretically predicted value of 0.25 itself indicates a deviation from the conditions of the renormalized Rouse model which have been shown experimentally to be fulfilled for isotropic melts [35]. Deviations from the bulk behavior can occur due to several factors such as changes in the chain topology, chain conformations, relative weight of long chain modes etc. Some of these factors are discussed below. However, it should be noted that either of these factors or even all of them can be responsible for the change in relaxation dispersion behavior.

The bulk behavior of entangled polymer melts, i.e. renormalised Rouse behavior is predicted for three-dimensional entangled polymers, but obviously, adsorbed polymer thin films cannot be treated as 3D melts in general. In fact, this study gives hints as to when this deviation becomes noticeable. One possible explanation can be sought in the relative im-

portance of entanglements: while PDMS30k is only marginally above the critical molecular weight (M_c=25 000) for the onset of entanglements, i.e., the crossover from Rouse to renormalized Rouse dynamics, PDMS200k has a much larger number of entanglements per chain. The lower molecular weight might thus more likely be affected by a change in topology, and entanglement effects could become inefficient near the surface. This would not be the case for PDMS200k. However, the behavior of relaxation dispersion of all molecular weight batches of PDMS under study show a similar dependence on polymer amount, with the thinnest layers being significantly affected. Apart from this, the fact that deviations from bulk behavior are also seen for PDMS10k thin films clearly shows that this is not a simple consequence of entanglement effects alone. Such a behavior can then be expected when the contributions from chain modes to the relaxation dispersion, mainly chain modes are affected due to a change in topology, which in turn results in a change in the dispersion slope.

Secondly, it can be observed that deviations in films occur when the layer thickness is smaller than R_g. Additionally these deviations depend only weakly on the molecular weight. For instance, PDMS 10k and 30k films show deviant relaxation dispersions when the film thickness obeys $d<0.2*R_g$ and $d<0.5*R_g$ respectively (such an observation was not possible for the highest molecular weight 200k, since films of higher thicknesses were technically difficult to prepare, due to the high solution viscosity). Chain conformations have been known to deviate from the bulk (Gaussian) in thin films of similar dimensions [69], where the changes affect the chain density and the excluded volume effects. This results in a change in inter-, intra-segmental and inter-molecular interactions. As was discussed above, the frequency regime being probed corresponding to limit II of renormalized Rouse model, the contributions are dominated by intra-segmental interactions. The above mentioned changes results in a different contribution to the relaxation dispersions resulting in a change in the dispersion shape. Additionally, this threshold thickness at which chains show deviation from bulk relaxation behavior may also directly relate to the thickness of the ARL.

The third possibility of this deviation could be due to a lesser weight of contributions

of long chain modes to the relaxation dispersion. The weaker contribution can stem from either or both of the above mentioned contributions, but this is the most straightforward explanation. If these contributions are less compared to bulk, then the dispersion shape is altered, and a deviation is observed. Given that even the thicker films of PDMS200k show deviation from the bulk slope might be substantive proof of the changing relative weight of chain modes specially at low frequencies.

The transverse relaxation times measured using solid echo give vital information supporting this model. While with increasing temperature, one sees an increase in the relaxation times expected for thermal processes such as segmental motion and chain modes, the more interesting information can be seen from the relative weight fraction of the components. Although it cannot be shown to be directly connected, the deviations in relaxation dispersion are accompanied by the short component amplitude of the solid echo decay curve being the major component(A^{SE}_{short} >0.5). For instance, deviations from bulk are observed at all temperatures for the PDMS30k - 1.25 nm layer film while the A^{SE}_{short} is the major component ($A^{SE}_{short} > A^{SE}_{long}$); for the 4.5 nm, relaxation dispersion is bulk like, and A^{SE}_{short} <A^{SE}_{long}. In a similar way for the 2.1 nm layer, where the dispersion approaches bulk-like behavior at higher temperature the A^{SE}_{short} also approaches being the minor component. Thus the A^{SE}_{short} could be a parameter directly accessing the fraction of ARL, while the relaxation time accessing the mobility. It is however to be remembered that there are more components much longer consisting of uncoupled mobile spins as studied by CPMG.

7.5 Conclusions

The dynamical behavior of PDMS thin films of varying molecular weight, both above and below the critical molecular weights, inside porous alumina of two different pore sizes (20 and 200 nm diameter) were investigated using NMR field cycling relaxometry, transverse relaxometry and ^{1}H Double Quantum NMR. The system represents a flexible polymer weakly adsorbed on a metal oxide surface leading to motional heterogeneities.

Relaxation dispersion of the films show that while fast reorientation motions are only weakly affected, slower motions appear to be more affected for all films. At thicknesses approaching the molecular size (R_g), the relaxation dispersion shows deviations from bulk, however, in other cases shows only a reduction in T_1 times with no qualitative deviation from bulk. The results show that the pore curvature to have a strong effect on the topology and hence the dynamic properties of the chains, as seen from the results; while films of 1-2 monolayer thickness in 200 nm pores show deviation from bulk, even the sub-monolayer films in 20 nm pores behave bulk-like. Due to the larger curvature in smaller pores considering the molecule size, the low energy of cohesion and the high energy of spreading state favors bulk-like layer. The curved surface of 200 nm pores however is large enough compared to the size of the molecules, for the films to spread and behave like a flat film. The mobility of the chains segments, in general, decreases with decreasing layer thickness as seen from transverse relaxation measurements. However, the motional restrictions are low compared to PDMS chains grafted to silica that are pinned to the surface, implying chains are not rigidly bound but relatively mobile, as expected for a weakly adsorbed polymer.

Most of the results can be interpreted on the basis of a two-component model. The thickness of the layer is divided into two regions, one closest to the surface, where chain mobility is affected by adsorption named *adsorption restricted layer*(ARL) and another region farther from the surface where chain mobility is affected only by chain connectivity (named *connectivity affected layer* or CRL). Chains in both the regions are dynamically hindered but chains in ARL show non-bulk behavior. The thickness of the layer is of the order of the minimum thickness below which deviations from bulk behavior appear in relaxation dispersion. The significance of this is that, the relaxation measurements made on this system are a manifestation of the contributions from the two regions. The spin-lattice relaxation, for instance, is an unresolved convolution of contributions from the regions; when the effects from non-bulk chains from ARL dominate, the dispersion deviates from bulk (Rouse and renormalised Rouse) behavior. Solid echo decay components appear to represent the frac-

tional weight of each component as seen from the short component that is dominant when deviation from bulk is seen in relaxometry profiles .

The deviations itself can be due to several factors that might be related, viz. (i) change in the 3D-topology of the film as the layer thickness decreases, affecting the inter- and intra-molecular interactions (ii) lower weightage of the long chain modes to the relaxation dispersion when compared to the bulk resulting in a change in the shape and (iii) changes in the chain conformation at very small thicknesses leading to a change in the interactions between segments leading to a deviant behavior. However, it should be noted that, although the latter has been observed in other systems, it could be far-fetched given that no direct investigations for proof of non-bulk conformations have been undertaken. Of the above factors, the first two seem to be the most plausible and direct explanations for the observed deviations.

Chapter 8

Conformation of a weakly adsorbed PDMS chain at an interface

8.1 Introduction

The structure and dynamics of surface molecules in confined systems is responsible for many of the mechanical properties. For instance, normal and frictional forces oscillate with the periodic dimensions of the chain, indicating layering in the films normal to the surface plane. Additional to layering, depending upon surface-specific interactions, the molecules may change their conformations to flat, extended shapes at the interfaces and orient partially or completely adjacent to the substrates. On an attractive surface, for instance, unentangled chains of a polymer melt are observed to orient parallel to the interface when sandwiched between two parallel impenetrable walls [89], and higher molecular weight chains have shown strong deviation from bulk conformations [90] at the interface. Conformational changes have been observed close to an interface formed with an attractive surface [2], specially when the length scale approaches the dimension of the bulk polymer gyration radius. [69]. While the nature of the interaction is well known to determine the adsorption strength, the dynamical aspects influencing the structure such as exchange, residential time, time-dependent fluctuations are not explicitly discussed, since most of the studied methods involve time averaging and are simply static in nature.

While PDMS chains have for long been speculated and observed to form flattened conformations [89, 75] even on non-interacting substrates [10], so far the discussions have not included dynamical aspects for the reasons just mentioned above. For instance, in weakly adsorbed systems, although flattened chains may exist, strong exchange between adsorbed and non-adsorbed molecules may cause a dynamic equilibrium even in monolayer and sub-monolayer thin films. Such information is either ignored or lost due to the intrinsic property of the measuring technique, specially due to vast differences in correlation times in the two states.

Using NMR relaxometry to investigate both the dynamics and structural aspects of such systems is well known [78, 84]. In this study, a popular but a less applied property of relaxation enhancement by paramagnetic spins is used to differentiate chains in the adsorbed

and non-adsorbed chains. Paramagnetic species contain one or more unpaired electrons possessing a positive magnetic susceptibility. These unpaired electron spins can strongly interact with nuclear spins enhancing the relaxation rates of the nuclear spins. This effect is called paramagnetic relaxation enhancement (PRE). This interaction is strongly dependent on the distance between the interacting (electron-nuclei) spins and by localizing the electron spins, distinction between spins that are close by and far away can be made.

Here, this property is used to distinguish between adsorbed and non-adsorbed chains as follows: The surface of the confining substrate is coated with paramagnetic species and ultrathin films are allowed to form on them. The relaxation rate of spins closest to the paramagnetic species, that is close to the surface are enhanced strongly, while the relaxation rate of spins that are far from the surface is either not enhanced or only slightly enhanced due to the paramagnetic species. A similar idea has been used by Gao et al [91] to study solubilizates in micellar systems by identifying solubilizates in the aqueous part where the paramagnetic ions exist. Here, by studying the fraction of adsorbed segments in films with thicknesses ranging from several monolayers to sub-monolayers, it is tried to verify if the chains indeed exist in flattened conformations, and if not, the consequential underlying reasons for such observations are explained. If flattened conformations do exist in this system at sub-monolayer thickness, one expects a mono-exponential component with the relaxation rate strongly enhanced.

8.2 Experiment

PDMS thin films of various thicknesses both in alumina (native) membranes and paramagnetic spin doped alumina (doped) membranes were prepared by dipping respective membranes in polymer solutions of various concentrations. More details of thin film preparation and characterization is detailed in §5.2.1. For preparing paramagnetic dopant coated alumina membranes, $Fe_2O_3.H_2O$ solution with a concentration of 8 mg/ml was used. The membranes after cleaning were left in the solution for not more than 3 minutes and imme-

diately after, rinsed in clean water to remove excess ferric oxide. The membranes were then evacuated overnight at around 100 °C, then the same procedure adopted for coating the native membranes was followed to form thin films from solution.

Table 8.1 : *PDMS30k thin films in alumina pores, precoated with paramagnetic ions. The nominal layer thickness was calculated as explained in §5.2.1. The surface coverage of Fe^{3+} ions was estimated to be ca. 0.6 mg/m^2.*

Pore specification	Avg. wt. of membranes (mg)	Avg. wt. of poly/mem (mg)	Nominal film thickness (nm)
Fe200	77.90	6.40	5.2
Fe200	80.72	3.80	3.0
Fe200	84.33	2.14	1.7
Fe200	82.20	1.95	1.4
Fe200	78.44	0.90	0.5

8.3 Results and Discussion

The longitudinal relaxation curves obtained for some of the PDMS30k samples in native A200 pores without any paramagnetic coating at 200 MHz are given in fig.8.1. As seen in the previous chapter, the relaxation curves are best described by a single exponential decay function, while higher order exponentials either resulted in unreasonable values and/or did not reduce the residuals significantly. The single exponential behavior is a result of long T_1 that allows better mixing as well as motional averaging due to fast segmental motion probed at these high fields. The same curves for the thin films in alumina pores coated with paramagnetic ions (doped pores) are shown in fig.8.2. The recovery curves obviously are non mono-exponential as seen from the fits (dashed lines) but rather bi-exponential (solid lines).

In fig.8.3, the relaxation times of thin films formed both in native alumina pores as well as doped pores, after analysis of the relaxation curves are shown. Alongside, the bulk relaxation values of PDMS30k melt is given by the horizontal line. Of the two components, the short component of thin films in doped alumina is not observed in native alumina pores

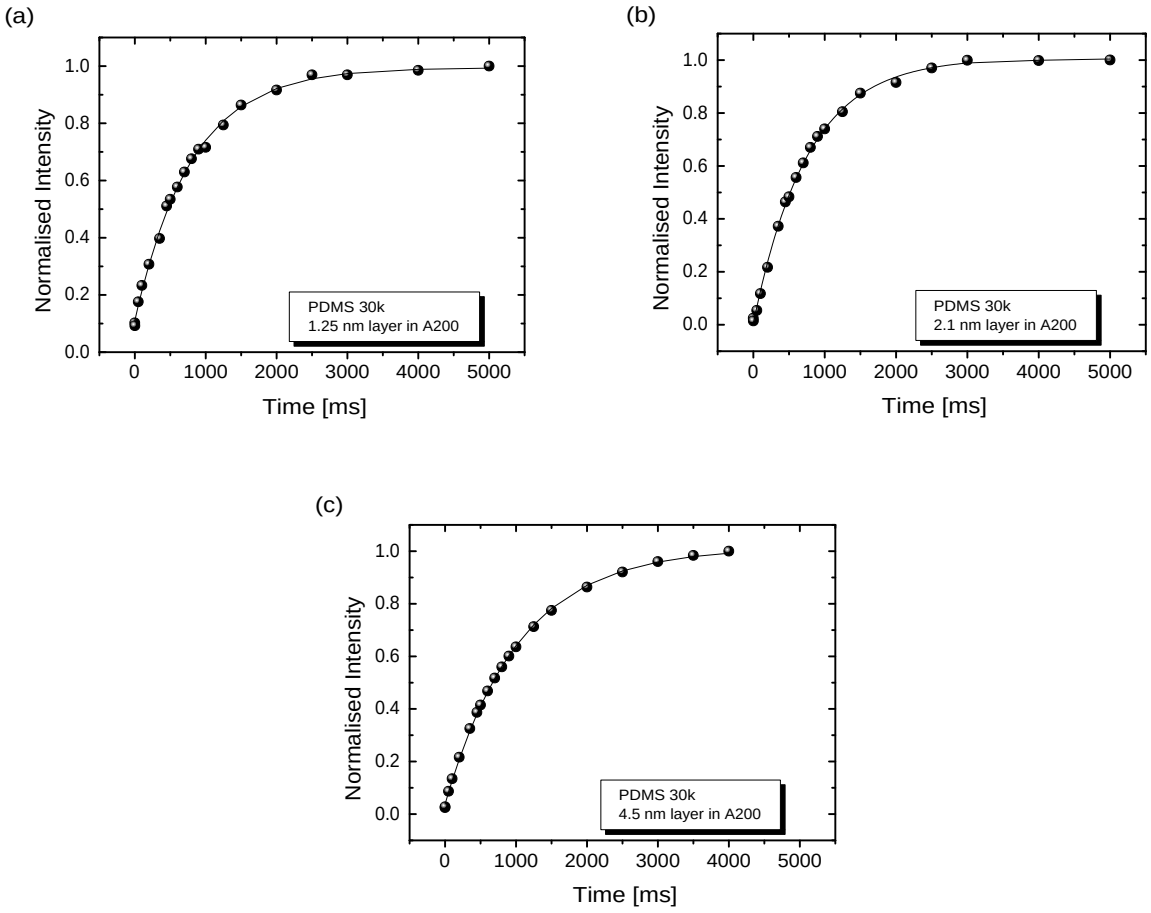

Figure 8.1 : *Longitudinal relaxation curves of PDMS30k thin film in un-doped porous alumina of various layer thicknesses(a)1.25 nm, (b)2.1 nm layer and (c)4.5 nm layer. Best fits to the curve using a mono-exponential decaying function are shown as solid lines in the figures.*

while the long component is comparable yet slightly shorter than the only component of thin films in native pores. Paramagnetic ions present only on the surface act as a relaxation sink hence enhance the relaxation rate of the spins in close proximity. Thus, the short component must arrive from chains that are in contact with the paramagnetic ions, which in turn are situated on the surface. The longer component then corresponds to the fraction that is not in contact or close to the surface. It is assumed that this component is not influenced by the paramagnetic ions on the pore surface. However the slight reduction in the T_1 is a result of the large sphere of influence of the paramagnetic effect of the ions [24]. Yet, assuming that this has no influence is reasonable considering (i)the high absolute value of

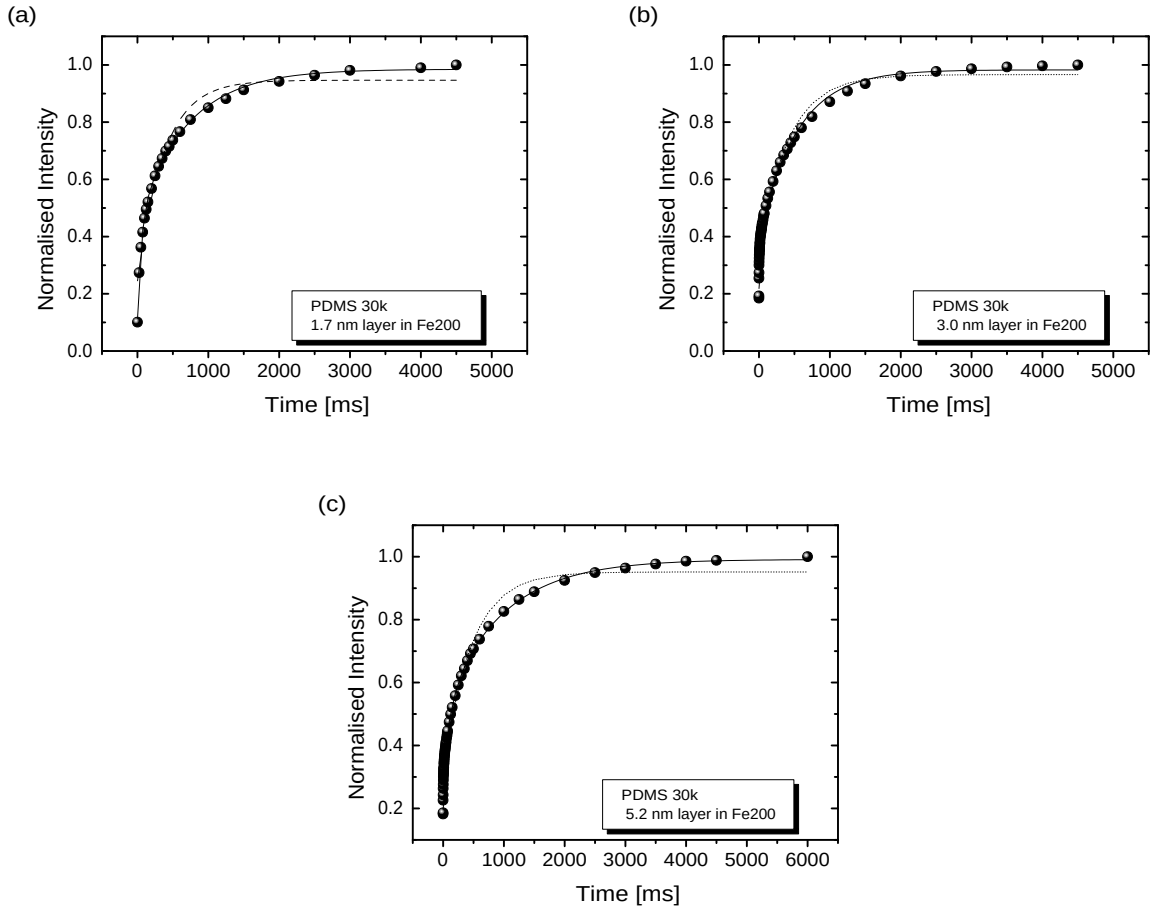

Figure 8.2 : *Longitudinal relaxation curves of PDMS30k thin film in porous alumina coated with paramagnetic ions of various layer thicknesses (a)1.7 nm layer, (b)3.0 nm layer and (c)5.2 nm layer. Best fits of bi-exponential function (solid line) and mono-exponential function (dashed line) are shown. Clearly the recovery is non-monoexponential.*

this component, (ii)the natural affinity of the ions to the hydrophilic alumina surface and hence a low probability that the ions dissolve in the polymer and (iii) the slow diffusion expected for a heavy ion in a viscous medium. Additionally such an influence does not interfere with the objective of the study, which is to distinguish between the two states.

The weight fraction of the short component constantly increases with decreasing layer thickness indicating increasing surface chains. Additionally there is up to a 3 folds decrease in the short component relaxation time with decreasing layer thickness. This has to be related to decreasing mobility with increasing confinement effect and/or increasing spin-paramagnetic species contacts. However, such a distinction is not clearly observed for the

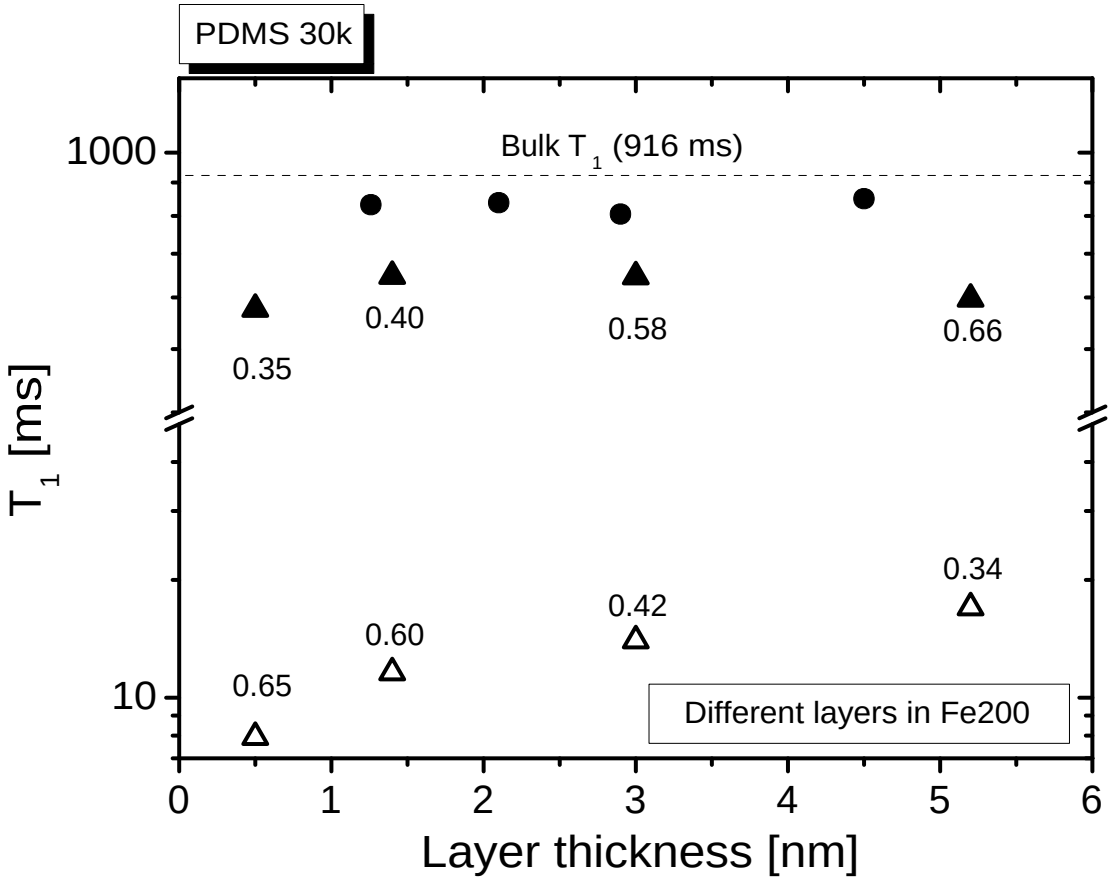

Figure 8.3 : *Comparison of relaxation times at 200 MHz of doped and un-doped samples of PDMS30k thin films. The horizontal line is the relaxation time of the bulk.*

longer component similar to relaxation in thin films inside native pores.

In summary, the shorter component arrives from surface adsorbed chains (and chains that are close to the surface), while the other component arrives from non-surface chains. The important aim of the study is to see how these surface chains are distributed at extremely low thin films or more precisely, at mono and sub-mono layer level thin films.

The sample with layer thickness 0.5 nm is nominally a sub-monolayer thin film. However, as observed on several other studies [76, 75] if the chains forms flattened conformations, the decay curve should be mono-exponential, with only the short component being observable. However the existence of two components, non-mono exponential behavior is in contrary

to this claim, at first glance. While the results observed here, correspond to only a major fraction of surface chains, not corresponding to flattened chains or chains located completely on the surface, there may be a lot of factors influencing the results.

Under exchange conditions between surface and non-surface chains, with a short residential time, the longitudinal relaxation time in native pores becomes weight averaged, but the fast relaxation due to paramagnetic ions at the surface renders only partial averaging leading to two components. Additionally, the curved surface may increase the energy of flattened conformations, thus the conformation observed on flat substrates may not be observed on curved surfaces even at sub-mono layer thicknesses.

8.4 Conclusions

Flattened conformations of PDMS chains have either been observed or predicted on different substrates using different methods. Here, a paramagnetic relaxation agent was used to differentiate between chains adsorbed on surface and non-adsorbed, where the paramagnetic species is present only on the surface. As per the other studies, at monolayer level or sub-monolayer level films, the component that is not influenced by paramagnetic species should be absent, however it is not the case. The intrinsic dynamic exchange between the chains in adsorbed and non-adsorbed chains in weakly adsorbed systems and the effect of a curved surface that induces additional energy for flat conformations are discussed as some of the main reasons.

Chapter 9

Summary and Outlook

Field cycling relaxometry was used to study polymer thin films formed inside porous substrates of different sizes. The frequency dependence of proton longitudinal relaxation times studied here, directly probe the spectral density function of motion in these thin films. The thickness of the film was varied in the range from several monolayers to sub-monolayer. In all cases, a slowing down of motion as reflected by lower relaxation times compared to bulk was observed, and a qualitative deviation from bulk occurred in cases of strong confinements.

Two different polymers, viz. PDMS and PB were used in this study. Porous alumina substrates and porous silica rods were used as confining substrates. The substrates differed in the pore size as well as affinity towards the polymer. The relaxation dispersion of the nominal thin layers formed in the pores were analyzed with reference to the relaxation dispersion of the bulk that followed model theories of polymer dynamics. Other than relaxation dispersion, transverse relaxometry and double quantum NMR was used in the study as a complementary technique to support the findings.

PB melt thin films were studied in porous alumina membranes as well as in porous silica rods. The molecular weight of PB used in the study was below the entanglement critical molecular weight ($M_w < M_c$). In bulk, the relaxation dispersion of the melt followed Rouse dynamics, as was evident from the master curve. The alumina pores certainly exceeded the molecular size of the polymer, while the silica pores were slightly smaller than the molecular size, hence the size effect is much different in the different pores as seen from the results. The findings of the study of PB layers in different pores are summarized below:

- The relaxation dynamics of thin films formed in alumina pores showed progressively increasing motional restrictions as the layer thickness decreased. Fast segmental reorientation motions probed at high frequencies were less affected compared to slower motions probed at lower frequencies. Yet, a qualitative deviation from bulk was not observed even for the thinnest (nominally sub-monolayer) films. It was shown that the poor wetting properties of the melt with alumina plays a major role. This directly affected the layer formation process, preventing the formation of a flat layer, with the nominal thickness, but forming blob with bulk-properties. This effect was enhanced in smaller pores, where the strong curvature inhibited the layer forming process further.

- The PB thin films formed in Vycor showed stronger motional restrictions. With the molecular size being larger than the pore, strong size effects were seen. The chains showed strong deviations from bulk, and showed a tendency to follow reptation behavior. However, in order to ascertain this, more information is needed on the interactions of the polymer with the surface.

- Studies of effect of polymer loading in Vycor demonstrated that as the amount of polymer loading decreased so did the motional restrictions owing to the increased motional degrees of freedom.

PDMS melts with three different molecular weights were used in the study; the molecular weights corresponding to below, above, and highly above the critical molecular weight. In bulk, the low molecular weight melt followed Rouse model and the other two molecular weights forming entanglements, followed renormalized Rouse ansatz. Although, manifestations due to confinement effect could be similar, the underlying processes can be different for the different molecular weights, especially on the lowest molecular weight that does not form entanglements.

Thin films of varying thicknesses were formed inside alumina pores of two different diameters. The nominal thickness of the films ranged from several monolayers to sub-monolayer levels. However, sub-monolayer level films were investigated only inside smaller pores. Field cycling relaxometry investigations were complemented with transverse relaxation and double quantum measurements. The findings of the various investigations are summarized below:

- The mobility of the thin films of all thicknesses were considerably reduced depending on the thickness. Like PB, fast segmental reorientation motions were less affected compared to the slower motions at lower frequencies that correspond to chain modes in bulk. The degree to which motions at high frequencies were affected showed a tendency of pore size dependence, at least for the low molecular weight.

- Chains below a certain thickness, defined by the radius of gyration, showed deviation from bulk behavior in terms of an increased power law behavior in the relaxation dispersion. These deviations are due to a different weight of the chain mode contributions to the relaxation times than in the bulk. The different contributions can arrive from either a change in the 3D-topology of the melt at such thicknesses or due to change in the conformations of the change in the film or both.

- A model based on the different measurements characterizing the chains in the layer is proposed. The layer thickness is divided into two layers, the *adsorption restricted layer* and the *connectivity restricted layer*. All measurements derive contributions from the two layers. The T_1 are an unresolved convolution of contributions from these layers. Deviation from the bulk in relaxation dispersion are seen when contributions from ARL dominate. Information about ARL can be arrived at from transverse relaxation measurements. The fraction of the ARL is given by the weight fractions of the

two components from solid echo decay. The thickness of ARL is of the order of the layer thickness below which deviations from bulk behavior are discerned in relaxation dispersions.

PDMS monolayers are known to form flattened conformations on both solid and liquid (non-curved) surfaces as studied by different static techniques. In the final study, surface conformations at monolayer level thicknesses were investigated using paramagnetic relaxation enhancement techniques to discriminate between surface and non-surface chains.

- The study did not conclusively prove that flattened chains exist in the system even at sub-monolayer thicknesses. However different factor that could lead to such a scenario are discussed including uneven distribution of paramagnetic species and weak adsorption strength of the polymer with the substrate leading to fast dynamic exchange between adsorbed and non-adsorbed segments.

The above studies have led to a phenomenological understanding of the effect of motional restrictions on polymer chains in thin films, due to film thickness and confinement (size effects), curvature of the pore (interfacial effect) and adsorption (surface interactions). The above mentioned effects on dynamics have been dealt with qualitatively in comparison to the melt dynamics, but a quantitative approach based on molecular simulations can help advance the understanding of these interesting and highly applied systems. It appears that the surface interactions play a major role in the dynamics of the system. Thus polymers with different affinity to the pores, as well as pores of different material can be used in the investigation. Nevertheless, more information can be extracted based on the surface interactions.

In addition to the techniques used above, other NMR techniques such as multi-nuclear NMR, solid-state NMR techniques such as multiple-quantum NMR, MAS techniques can be used to get important information.

References

[1] Forrest, J., DalnokiVeress, K., Stevens, J. & Dutcher, J. *Phys. Rev. Lett.* **77**(10), 2002 (1996).

[2] Kraus, J., Muller-Buschbaum, P., Kuhlmann, T., Schubert, D. W. & Stamm, M. *Europhysics Letters* **49**(2), 210 (2000).

[3] Domke, J. & Radmacher, M. *Langmuir* **14**(12), 3320 (1998).

[4] Kajiyama, T., Tanaka, K. & Takahara, A. in *Symposium on Metastability and Critical Phenomena in Polymers and Polymer Phase Transitions at the Spring Materials-Research-Society Meeting*, volume 39, 4665.

[5] Luengo, G., Schmitt, F. J., Hill, R. & Israelachvili, J. *Macromolecules* **30**(8), 2482 (1997).

[6] Schmitt, J. *et al. Macromolecules* **26**(25), 7058 (1993).

[7] Orts, W. J., Vanzanten, J. H., Wu, W. L. & Satija, S. K. *Phys. Rev. Lett.* **71**(6), 867 (1993).

[8] Fukao, K. & Miyamoto, Y. *Phys. Rev. E* **61**(2), 1743 (2000).

[9] Zeghal, M., Deloche, B. & Auroy, P. *Macromolecules* **32**(15), 4947 (1999).

[10] Rivillon, S., Auroy, P. & Deloche, B. *Phys. Rev. Lett.* **84**(3), 499 (2000).

[11] Primak, S. V., Jin, T., Dagger, A. C., Finotello, D. & Mann, E. K. *Phys. Rev. E* **65**(3) (2002).

[12] Noack, F. *Prog. Nucl. Magn. Reson. Spectrosc.* **18**, 171 (1986).

[13] Kimmich, R. & Anoardo, E. *Prog. Nucl. Magn. Reson. Spectrosc.* **44**, 257 (2004).

[14] McLeish, T. *Advances in Physics* **51**(6), 1379–1527 (2002).

[15] Rouse, P. *J. Chem. Phys.* **21**(7), 1272 (1953).

[16] Zimm, B. *J. Chem. Phys.* **24**(2), 269 (1956).

[17] De Gennes, P. G. *J. Chem. Phys.* **55**(2), 572 (1971).

[18] Doi, M. & Edwards, S. *Theory of polymer Dynamics*. Clarendon Press, Oxford, (1986).

[19] Schweizer, K. S. *J. Chem. Phys.* **91**(9), 5802 (1989).

[20] Kimmich, R. & Fatkullin, N. *Advances in Polymer Science* **170**, 1 (2004).

[21] Ernst, R., Bodenhausen, G. & Wokaun, A. *Principles of Nuclear Magnetic Resonance in One and Two dimensions*. Clarendon Press, Oxford, (1987).

[22] Levitt, M. *Spin dynamics: Basics of Nuclear magnetic resonance., 2nd edition*. Wiley & Sons, West Sussex, (2008).

[23] Kimmich, R. *NMR Tomography, Diffusometry, Relaxometry*. Springer, Berlin, (1997).

[24] Fukushima, E. & Roeder, S. *Experimental Pulse NMR: A Nuts and Bolts Approach*. Addison-Wesley, London, (1981).

[25] McBrierty, V. & Packer, K. *Nuclear Magnetic Resonance in Solid Polymers*. Cambridge University Press,Cambridge, (2006).

[26] Bloch, F. *Phys. Rev.* **70**(7), 460 (1946).

[27] Bloembergen, N., Purcell, E. M. & Pound, R. V. *Phys. Rev.* **73**(7), 679 (1948).

[28] Kingsley, P. B. *Conc. in Magn. Reson.* **11**(4), 243 (1999).

[29] Hahn, E. L. *Phys. Rev.* **80**(4), 580 (1950).

[30] Carr, H. & Purcell, E. *Phys. Rev.* **94**(3), 630 (1954).

[31] Meiboom, S. & Gill, D. *Review of Scientific instruments* **29**(8), 688 (1958).

[32] Powles, J. G. & Mansfield, P. *Physics Letters* **2**(2), 58 (1962).

[33] Abragam, A. *Principles of Nuclear Magnetism*. Clarendon Press, Oxford, (1961).

[34] Fatkullin, N., Kimmich, R. & Weber, H. *Phys. Rev. E* **47**(6), 4600 (1993).

[35] Weber, H. W. & Kimmich, R. *Macromolecules* **26**(10), 2597 (1993).

[36] Fatkullin, N. & Kimmich, R. *J. Chem. Phys.* **101**(1), 822 (1994).

[37] Kimmich, R., Fatkullin, N., Seitter, R. & Gille, K. *J. Chem. Phys.* **108**(5), 2173 (1998).

[38] Gubaidullin, A., Shakirov, T., Fatkullin, N. & Kimmich, R. *Solid state Nuclear Magnetic resonance* **35**(3), 147 (2009).

[39] Mattea, C. *et al. Appl. Magn. Reson.* **27**(3-4), 371 (2004).

[40] Denissov, A., Kroutieva, M., Fatkullin, N. & Kimmich, R. *J. Chem. Phys.* **116**(12), 5217 (2002).

[41] Kausik, R., Mattea, C., Fatkullin, N. & Kimmich, R. *J. Chem. Phys.* **124**(11), 114903 (2006).

[42] Grössl, G., Winter, F. & Kimmich, R. *J. Phys. E: Sci. Instrum.* **18**(4), 358 (1985).

[43] Schweikert, K.-H., Krieg, R. & Noack, F. *J. Magn. Reson.* **78**(1) (1988).

[44] Melton, B., Pollak, V., Mayes, T. & Willis, B. *J. Magn. Reson.* **A117**(2), 164 (1995).

[45] Pound, R. *Phys. Rev.* **81**, 156 (1951).

[46] Weitekamp, D., Bielecki, A., Zax, D., Zilm, K. & Pines, A. *Phys. Rev. Lett.* **50**, 1807 (1983).

[47] Redfield, A., Fite, W. & Bleich, H. *Rev. Sci. Instrum.* **39**(5), 710 (1968).

[48] Kimmich, R. & Noack, F. *Z. Angew. Phys.* **29**, 248 (1970).

[49] Ferry, J. *Viscoelastic properties of Polymers.* Wiley, New York, (1980).

[50] Bailey, R., North, A. & Pethrick, R. *Molecular motion in High Polymers.* Clarendon, Oxford, (1981).

[51] Platt, M., Dryfe, R. & Roberts, E. *Langmuir* **19**(19), 8019 (2003).

[52] Okuom, M. O., Metin, B. & Blum, F. D. *Langmuir* **24**(6), 2539 (2008).

[53] Slichter, C. *Principle of Magnetic Resonance, 3rd edition.* Springer, Berlin, (1980).

[54] Saalwaechter, K. *Prog. Nucl. Magn. Reson. Spectrosc.* **51**(1), 1 (2007).

[55] Schneider, M., Demco, D. E. & Blumich, B. *Macromolecules* **34**(12), 4019 (2001).

[56] Wiesmath, A., Filip, C., Demco, D. E. & Blumich, B. *J. Magn. Reson.* **154**(1), 60 (2002).

[57] Kimmich, R. *et al. J. Chem. Phys.* **107**(15), 5973 (1997).

[58] Kariyo, S. & Stapf, S. *Macromolecular Chemistry and Physics* **206**(13), 1300 (2005).

[59] Kausik, R., Mattea, C., Kimmich, R. & Fatkullin, N. *Eur. Phys. J.-Spec. Top.* **141**, 235 (2007).

[60] Stapf, S. & Kimmich, R. *Macromolecules* **29**(5), 1638 (1996).

[61] Tsige, M. *et al. J. Chem. Phys.* **118**(11), 5132 (2003).

[62] Stapf, S. & Kimmich, R. *Macromolecules* **29**(5), 1638 (1996).

[63] Kausik, R., Fatkullin, N., Huesing, N. & R., K. *Magn. Reson. Imaging.* **25**, 489 (2007).

[64] Pearson, D. & Helfand, E. *Macromolecules* **17**(4), 888 (1984).

[65] Klein, P. G. *et al. Macromolecules* **31**(25), 8871 (1998).

[66] McGuiggan, P. M., Gee, M. L., Yoshizawa, H., Hirz, S. J. & Israelachvili, J. N. *Macromolecules* **40**(6), 2126 (2007).

[67] Kariyo, S. *Molecular dynamics of polymers by means of NMR field cycling relaxometry.* PhD thesis, RWTH-Aachen University, (2005).

[68] Fatkullin, N., Kausik, R. & Kimmich, R. *J. Chem. Phys.* **126**, 094904 (2007).

[69] Jones, R. L., Kumar, S. K., Ho, D. L., Briber, R. M. & Russell, T. P. *Nature* **400**(6740), 146 (1999).

[70] Wallace, W., Vanzanten, J. & Wu, W. *Phys. Rev. E* **52**(4A), R3329 (1995).

[71] Keddie, J., Jones, R. & Cory, R. *Europhysics Letters* **27**(1), 59 (1994).

[72] Zheng, X. *et al. Phys. Rev. Lett.* **74**(3), 407 (1995).

[73] Zheng, X. *et al. Phys. Rev. Lett.* **79**(2), 241 (1997).

[74] O'Shaughnessy, B. & Vavylonis, D. *Journal of Physics-Condensed Matter* **17**(2), R63 (2005).

[75] Lee, L. T. *et al. Macromolecules* **26**(25), 7046 (1993).

[76] Daillant, J., Benattar, J. J. & Leger, L. *Phys. Rev. A* **41**(4), 1963 (1990).

[77] Jagadeesh, B., Demco, D. E. & Blumich, B. *Chem. Phys. Lett.* **393**(4-6), 416 (2004).

[78] Litvinov, V. M., Barthel, H. & Weis, J. *Macromolecules* **35**(11), 4356 (2002).

[79] Schneider, M., Gasper, L., Demco, D. E. & Blumich, B. *J. Chem. Phys.* **111**(1), 402 (1999).

[80] Kimmich, R., Seitter, R. O., Beginn, U., Moller, M. & Fatkullin, N. *Chem. Phys. Lett.* **307**(3-4), 147 (1999).

[81] Fatkullin, N., Fischer, E., Mattea, C., Beginn, U. & Kimmich, R. *ChemPhysChem* **5**(6), 884 (2004).

[82] Cosgrove, T., Prestidge, C. A. & Vincent, B. *Journal of the Chemical Society-Faraday Transactions* **86**(9), 1377 (1990).

[83] Douglas, J. F., Schneider, H. M., Frantz, P., Lipman, R. & Granick, S. *J. Phys.-Condes. Matter* **9**(37), 7699 (1997).

[84] Cosgrove, T., Roberts, C., Garasanin, T., Schmidt, R. G. & Gordon, G. V. *Langmuir* **18**(26), 10080 (2002).

[85] DeMaggio, G. B. *et al. Phys. Rev. Lett.* **78**(8), 1524 (1997).

[86] Napolitano, S. & Wubbenhorst, M. *J. Phys. Chem. B* **111**(21), 5775 (2007).

[87] Napolitano, S. & Wubbenhorst, M. *J. Phys. Chem. B* **111**(31), 919 (2007).

[88] Rittigstein, P., Priestley, R., Broadbelt, L. & Torkelson, J. *Nature Materials* **6**(4), 278 (2007).

[89] Evmenenko, G., Dugan, S., Kmetko, J. & Dutta, P. *Langmuir* **17**(13), 4021 (2001).

[90] Seo, Y. *et al. Phys. Rev. Lett.* **94**(15) (2005).

[91] Gao, Z., Wasylishen, R. E. & Kwak, J. C. T. *J. Phys. Chem* **93**, 2190 (1989).

Publications by the author

1. Ayalur-karunakaran,S., Blümich,B. and Stapf,S.,
   NMR investigations of polymer dynamics in a partially filled porous matrix,
   Eur. Phys. J. E 26(20), 43 (2008).

2. Ayalur-Karunakaran, S., Blümich, B., and Stapf,S.,
   Chain Dynamics of a Weakly Adsorbing Polymer in Thin Films,
   Langmuir 25 (26), 12208 (2009).

Acknowledgements

First, my heartful thanks goes to my supervisor Siegfried Stapf for his continuing supporting my PhD. His encouragement for being independent yet lending a helping hand everytime when it was needed. His perseverance and push in making me work towards a goal has helped me hone every skill I possess. I am very thankful to Prof. Blümich for allowing me to carry out my Doctoral work in his lab and for his advice and interest in my work. He made the whole stay, a very pleasant one. Another person that i am equally indebted to is Prof.Demco, from whom I drew a lot of inspiration out of his youthful enthusiasm about science. How grateful I feel for what I gained from the discussions I had with him, cannot be expressed with words.

I would like to express my sincere thanks to Marko (Bertmer), Alina (Buda-Adams), Adi (Mihai Adrian) Voda and Andrea Amar who were very helpful in helping me orient with high field NMR specially in the initial days. Marko, additionally for many fruitful theoretical student-teacher discussions. I would also like to express my thanks to Federico Casanova, with whom i had several useful discussions, specially during the mid-part of my thesis. I am equally grateful to Rudra Choudhury not only for the numerous discussions we had in the office but for his constant encouragement, care and friendship. A special reservation of thanks to Markus Küppers and Jörg Mauler who helped me in both professional and personal ways on many many things. In this aspect, I am equally indebted to Rainer Haas 'the google and Wikipedia of ITMC', without whom I wouldn't have been able to accomplish many things I did during sample preparation.

DWI is gratefully acknowledged for letting me to use their labs for experimental purposes.

I am very thankful to Dr.Ahmed Mourran who helped make the contact angle measurements and other AFM measurements. Special thanks to Metodi Bozukov, Marko Backes and Priya Garg for helping me with the glasswares, vacuum pump and vycor sample preparation preparation. Thanks to Michael Adams for the time he spent with the FFC, specially for changing the MOSFETs among other things. Consultations from Matteo Pollelo from Stelar S.r.l. is also gratefully acknowledged. Help from Klaus Kupferschlaeger is also gratefully acknowledged. For keeping the nice atmosphere that is the group, I would like to thank all of my colleagues who were always nice through thick and thin. Special thanks to Rudra, Joerg, Dora, Juergen, Tsolmon, Lavinia and Elena. Finally, the most special thanks to the people who stood through the thick and thin time by side: my parents, Gilda and also to all my friends back home, who were constantly helping me and for being there whenever i needed any help.